

This peer-reviewed published paper appears as: Hwang, S.-H., Lignos, D.G. (2017). “Effect of Modeling Assumptions on the Earthquake-Induced Losses and Collapse Risk of Steel-Frame Buildings with Special Concentrically Braced Frames”, *Journal of structural Engineering*, **143**(9), 04017116-1, DOI:10.1061/(ASCE)ST.1943-541X.0001851.

# Effect of Modeling Assumptions on the Earthquake-Induced Losses and Collapse Risk of Steel-Frame Buildings with Special Concentrically Braced Frames

Seong-Hoon Hwang<sup>1</sup>

Dimitrios G. Lignos, A.M. ASCE<sup>2</sup>

## ABSTRACT

This paper quantifies the collapse risk and earthquake-induced economic losses of steel-frame buildings with special concentrically braced frames designed in urban California. A probabilistic building-specific loss estimation methodology that can explicitly account for the main sources of variability related to seismic hazards and structural response is utilized for this purpose. It is shown that, depending on the choice of the loss-metric, at seismic events with low probability of occurrence (i.e., 2% probability of occurrence in 50 years), losses because of demolition and structural collapse in steel-frame buildings with special concentrically braced frames designed in highly seismic zones may be significantly overestimated when ignoring the contribution of the composite floor and gravity framing system to the analytical model building representation. For frequent and moderately frequent seismic events (i.e., 50 and 10% probability of exceedance over 50 years of building life expectancy), acceleration-sensitive nonstructural component repairs govern building losses regardless of the analytical model representation used. For the same seismic events, an appreciable contributor to total losses in steel-frame buildings with special concentrically braced

---

<sup>1</sup>Graduate Student, Dept. of Architecture, Civil and Environmental Engineering, Swiss Federal Institute of Technology, École Polytechnique Fédérale de Lausanne, EPFL ENAC IIC RESSLab, CH-1015 Lausanne, Switzerland; Dept. of Civil Engineering and Applied Mechanics, McGill Univ., Montreal, QC, Canada H3A 2K6. E-mail: seong-hoon.hwang@epfl.ch, seong-hoon.hwang@mail.mcgill.ca

<sup>2</sup>Associate Professor, Dept. of Architecture, Civil and Environmental Engineering, Swiss Federal Institute of Technology, École Polytechnique Fédérale de Lausanne, EPFL ENAC IIC RESSLab, CH-1015 Lausanne, Switzerland (corresponding author). E-mail: dimitrios.lignos@epfl.ch.

frames is structural repairs because of steel brace flexural buckling. It is suggested that dual-parameter rather than drift-based steel brace fragility curves should be used in loss computations conditioned on a single seismic intensity. Otherwise, the expected annual losses should be used as a metric for building-specific loss assessment of steel-frame buildings with special concentrically braced frames.

**Keywords:** Earthquake loss assessment; Collapse risk; Special concentrically braced frames; Losses because of demolition; Gravity framing; residual deformations; Seismic effects.

## INTRODUCTION

Steel concentrically braced frames (CBFs) are a widely used lateral load-resisting system around the world to withstand earthquake loading. Because of the steel brace's asymmetric hysteretic behavior in combination with a wide-range of CBF configurations, local story collapse mechanisms may develop because of plastic deformation concentrations. This could potentially result into large residual story deformations or structural collapse (Tremblay et al. 1995; Tremblay et al. 1996). The magnitude of residual deformations along the height of a building is likely to affect decisions associated with building demolition in the aftermath of an earthquake (Ramirez and Miranda 2012). During more frequently occurring earthquakes (i.e., service-level or design-basis earthquakes), steel CBFs may experience fairly high absolute acceleration demands because of the high lateral stiffness they can provide compared to other lateral load-resisting systems as well as the contribution of higher mode effects to the structural response (Rodriguez et al. 2002; Chopra 2011; Ray-Chaudhuri and Hutchinson 2011). Prior studies (Tremblay 2002; Roeder et al. 2012; Lignos and Karamanci 2013) have indicated that steel brace flexural buckling typically occurs, on average, at a story drift ratio (i.e., the ratio of the relative lateral displacement between two adjacent floors to the story height) of approximately 0.5%. Considering all the previous, steel CBFs may experience appreciable earthquake-induced losses because of damage in the structural and nonstructural building content at seismic intensities associated with design-basis earthquakes. Such losses should be quantified in a rational manner.

With the advent of performance-based earthquake engineering (PBEE) (Cornell and Krawin-

46 kler 2000; FEMA 2012), a number of studies quantified earthquake-induced losses mainly for con-  
47 ventional reinforced concrete (Mitrani-Reiser 2007; Ramirez et al. 2012; Baradaran Shoraka et al.  
48 2013) and wood structures (Porter et al. 2006; Pei and van de Lindt 2009). In a more recent study,  
49 Song et al. (2016) showed that the earthquake-induced losses of steel-frame buildings account-  
50 ing for mainshock-aftershock sequences are approximately 27–40% higher than those considering  
51 mainshocks only. Ramirez and Miranda (2012) pointed out that building demolition may become  
52 a controlling parameter in conventional modern building construction because of large residual de-  
53 formations. Liel and Deierlein (2013) showed that direct earthquake-induced losses in nonductile  
54 reinforced concrete buildings are only twice those for modern code-compliant buildings, whereas  
55 their collapse risk is on the order of at least 30 times higher than code-conforming buildings. To  
56 the best of the authors' knowledge, there has not been an attempt to quantify the structural and  
57 nonstructural repairs needed in steel-frame buildings with CBFs in the aftermath of an earthquake.  
58 This process is not trivial because it should explicitly consider the beneficial influence of gravity  
59 framing and column continuity on the distribution of story drift demands and reserve capacity of  
60 the steel-frame buildings (Gupta and Krawinkler 1999; MacRae et al. 2004; Ji et al. 2009; Stoakes  
61 and Fahnestock 2011; Fahnestock et al. 2014; Flores et al. 2014; Elkady and Lignos 2015; Flores  
62 et al. 2016); else, the estimated economic losses can be vastly overestimated (NIST 2012b).

63 Building-specific loss estimation methodologies are typically based on univariate (i.e., either  
64 drift- or acceleration-based) fragility curves for structural and nonstructural building components  
65 (Porter et al. 2001; FEMA 2012; Li and van de Lindt 2012). This is done in an effort to retain  
66 simplicity in the loss computations. However, damageable components may be very sensitive  
67 to other geometric and material parameters that are often ignored as part of the loss estimation  
68 process. Aslani and Miranda (2005) demonstrated that bivariate fragility curves are more suitable  
69 than drift-based fragilities to characterize slab-column connection damage in existing nonductile  
70 reinforced concrete buildings. In a more recent study, Lignos and Karamanci (2013) demonstrated  
71 the efficiency of dual-parameter fragility curves for building-specific loss estimation of steel CBFs.  
72 This is because of the influence of steel brace global and local slenderness on the predefined steel

73 brace damage states that are used within the current loss estimation methodologies.

74 This paper addresses all the aforementioned issues by evaluating the expected earthquake-  
75 induced losses in archetype steel-frame buildings with special concentrically braced frames (SCBFs)  
76 designed in urban California. The evaluation is conducted at various ground motion intensities un-  
77 til the occurrence of structural collapse. In this process, the influence of residual deformations on  
78 the building repairs is explicitly considered. Emphasis is placed on the effect of gravity framing  
79 and the selected steel brace fragility curve on the loss computations. The influence of the selected  
80 seismic design category on the earthquake-induced losses of steel-frame buildings with SCBFs is  
81 examined. Guidance on the selection of the appropriate loss-metric is also provided, depending on  
82 the seismic performance of interest.

## 83 **OVERVIEW OF SEISMIC LOSS ESTIMATION METHODOLOGY USED**

84 The main aspects of the used building-specific loss estimation methodology adopted from  
85 Ramirez and Miranda (2012) are summarized herein. This is a story-based building-specific loss  
86 estimation methodology in which engineering demand parameters (EDPs) at each story are com-  
87 puted based on nonlinear response history analysis. The methodology described below has been  
88 implemented in an interactive *MATLAB* routine (MATLAB 2015). By assuming mutually exclusive  
89 and collectively exhaustive events of building collapse and no collapse, the mean of total seismic  
90 losses in a frame building conditioned on the seismic intensity measure  $IM=im$  (i.e.,  $\mu_{L_T|IM}$ ) is  
91 described by,

$$92 \quad \mu_{L_T|IM} = \mu_{L_{NC}|IM,NC} (1 - P_{C|IM}) + \mu_{L_C|C} P_{C|IM} \quad (1)$$

93 where  $\mu_{L_{NC}|IM,NC}$  is the mean value of the loss conditioning on no collapse for a given  $IM=im$ ;  
94  $\mu_{L_C|C}$  is the mean value of the loss because of collapse (this is independent of seismic intensity  
95  $IM$ ); and  $P_{C|IM}$  is the collapse probability given an  $IM=im$ . Non-collapse losses  $\mu_{L_{NC}|IM,NC}$  can  
96 be further disaggregated into losses because of repairs for structural, drift-sensitive, acceleration-  
97 sensitive nonstructural components and demolition as discussed in Ramirez and Miranda (2012).

98 Therefore, Eq. (1) can be rewritten as,

$$99 \quad \mu_{L_T|IM} = \mu_{L_R|R,IM,NC} P_{R|IM,NC} (1 - P_{C|IM}) + \mu_{L_D|D,IM,NC} P_{D|IM,NC} (1 - P_{C|IM}) + \mu_{L_C|C} P_{C|IM} \quad (2)$$

100 where  $\mu_{L_R|R,IM,NC}$  is the mean of losses because of repairs for structural and nonstructural com-  
 101 ponents conditioned on no collapse given a seismic intensity  $IM=im$ ;  $\mu_{L_D|D,IM,NC}$  is the mean of  
 102 losses because of demolition conditioned on no collapse, given a seismic intensity  $IM=im$ ;  $P_{R|IM,NC}$   
 103 and  $P_{D|IM,NC}$  are the probabilities that the building is being considered to be repaired and be de-  
 104 molished, respectively, both conditioned on no collapse given a seismic intensity  $IM=im$ ; therefore,  
 105 Eq. (2) becomes,

$$106 \quad \mu_{L_T|IM} = \mu_{L_R|R,IM,NC} (1 - P_{D|IM,NC}) (1 - P_{C|IM}) + \mu_{L_D|D,IM,NC} P_{D|IM,NC} (1 - P_{C|IM}) + \mu_{L_C|C} P_{C|IM} \quad (3)$$

107 In this paper,  $\mu_{L_R|R,IM,NC}$  can be estimated by considering the discrete damage state a compo-  
 108 nent experiences by using Eq. (4),

$$109 \quad \mu_{L_R|R,IM,NC} = \sum_{i=1}^m \sum_{j=0}^n \int_0^{\infty} \mu_{L_{ij}|DS_{ij}} P_{DS_{ij}|EDP} f_{EDP|IM} dEDP \quad (4)$$

110 where  $m$  is the number of damageable components being considered;  $n$  is the number of damage  
 111 states a component may experience;  $\mu_{L_{ij}|DS_{ij}}$  is the mean repair cost for the  $i$ th component being  
 112 in the  $j$ th damage state;  $P_{DS_{ij}|EDP}$  is the probability of the EDP of interest associated with the  $i$ th  
 113 component being or exceeding the  $j$ th damage state given an  $EDP=edp$ ,

$$114 \quad P_{DS_{ij}|EDP} = \begin{cases} 1 - F_{DS_{i1}}(EDP) & \text{if } j = 0 \text{ (no damage)} \\ F_{DS_{ij}}(EDP) - F_{DS_{i(j+1)}}(EDP) & \text{if } 1 \leq j < n \\ F_{DS_{ij}}(EDP) & \text{if } j = n \end{cases} \quad (5)$$

115 where  $F_{DS_{ij}}$  is the fragility curve for the  $i$ th component being in the  $j$ th damage state, that is the

116 probability that the component of being or exceeding damage state  $ds$  conditioned on an EDP= $edp$   
 117 of interest; and  $f_{\text{EDP}|\text{IM}}$  is the probability density function of the EDP of interest given an IM= $im$ .

118 In the case in which dual-parameter fragility curves are used for a structural component (e.g.,  
 119 steel brace in this case) as part of the PBEE framework, Eq. (5) should be modified as follows  
 120 in order to take into account both the EDP and the considered geometric parameter (GP) of the  
 121 respective structural component,

$$122 \quad P_{\text{DS}_{ij}|\text{EDP,GP}} = \begin{cases} 1 - F_{\text{DS}_{i1}}(\text{EDP,GP}) & \text{if } j = 0 \text{ (no damage)} \\ F_{\text{DS}_{ij}}(\text{EDP,GP}) - F_{\text{DS}_{i(j+1)}}(\text{EDP,GP}) & \text{if } 1 \leq j < n \\ F_{\text{DS}_{ij}}(\text{EDP,GP}) & \text{if } j = n \end{cases} \quad (6)$$

123 where  $P_{\text{DS}_{ij}|\text{EDP,GP}}$  is the fragility curve of the structural component being in the  $j$ th damage state,  
 124  $ds$  conditioned on the EDP= $edp$  and the geometric parameter GP= $gp$  of interest;  $F_{\text{DS}_{ij}}(\text{EDP, GP})$   
 125 is the fragility curve that computes the probability of being or exceeding the  $j$ th damage state of  
 126 the  $i$ th structural component conditioned on the EDP= $edp$  and the geometric parameter GP= $gp$  of  
 127 interest (e.g., global or local slenderness). If the two random variables (i.e., EDP and GP) are  
 128 lognormally distributed, a joint probability distribution  $F_{\text{DS}_{ij}}(\text{EDP, GP})$  may be represented by a  
 129 bivariate lognormal distribution (Aitchison and Brown 1957). For steel braces, it was found that  
 130 the random variables of the dual-parameter fragility curves are statistically independent (Lignos  
 131 and Karamanci 2013); therefore, Eq. (6) is modified as follows,

$$132 \quad P_{\text{DS}_{ij}|\text{EDP,GP}} = \begin{cases} 1 - F_{\text{DS}_{i1}}(\text{EDP}) F_{\text{DS}_{i1}}(\text{GP}) & \text{if } j = 0 \text{ (no damage)} \\ F_{\text{DS}_{ij}}(\text{EDP}) F_{\text{DS}_{ij}}(\text{GP}) - F_{\text{DS}_{i(j+1)}}(\text{EDP}) F_{\text{DS}_{i(j+1)}}(\text{GP}) & \text{if } 1 \leq j < n \\ F_{\text{DS}_{ij}}(\text{EDP}) F_{\text{DS}_{ij}}(\text{GP}) & \text{if } j = n \end{cases} \quad (7)$$

133 where  $F_{\text{DS}_{i1}}(\text{EDP})$  is the fragility curve for the  $j$ th damage state of the  $i$ th structural component  
 134 conditioned on the EDP= $edp$  of interest; and  $F_{\text{DS}_{ij}}(\text{GP})$  is the fragility curve that computes the

135 probability of being or exceeding the  $j$ th damage state conditioned on the geometric parameter  
 136 GP= $gp$  of interest.

137 In order to estimate the probability that a building will be demolished given that it did not  
 138 collapse when subjected to an earthquake with seismic intensity IM= $im$ , the following relationship  
 139 can be used,

$$140 \quad P_{D|IM,NC} = \int_0^{\infty} P_{D|RSDR} f_{RSDR|IM} dRSDR \quad (8)$$

141 where  $f_{RSDR|IM}$  is the probability density function of the maximum residual drift ratio along the  
 142 height of the building, given an intensity measure IM= $im$ ;  $P_{D|RSDR}$  is the probability of having  
 143 to demolish the building conditioned on the maximum residual story drift ratio, RSDR, along the  
 144 height of the building, which is modeled by a lognormal distribution with a median,  $\mu_{D|RSDR} =$   
 145 0.015 radians and a logarithmic standard deviation,  $\beta_{\ln D|RSDR} = 0.3$  (Ramirez and Miranda 2012).  
 146 It should be noted that these parameters are based on engineering judgment and could vary in  
 147 different regions around the world. It is noted that the earthquake-induced loss computations are  
 148 based on story-based EDPs as proposed by Ramirez and Miranda (2012). Based on the same  
 149 methodology, in case that a residual drift concentrates in one (or few) story(ies) along the height  
 150 of a building then losses because of demolition are governed by this case.

151 The probabilistic seismic demand model should be determined to characterize the probabilistic  
 152 relationship between the EDP of interest associated with a measure of seismic demand in a frame  
 153 building [e.g., peak story drift ratios (SDRs), peak absolute floor accelerations (PFAs), residual  
 154 story drift ratios (RSDRs), etc.] and the seismic intensity IM= $im$  during the earthquake event. This  
 155 model is intended for the integration process over the entire range of EDPs to be used in the compu-  
 156 tations of the earthquake-induced economic losses. In this paper, the probability density functions  
 157 of attaining a specified structural demand of interest given an IM= $im$  (i.e.,  $f_{EDP|IM}$ ) are assumed  
 158 to follow a lognormal distribution defined by the median  $\mu_{EDP|IM}$  and the logarithmic standard  
 159 deviation  $\beta_{\ln EDP|IM}$  of the parameters. The parametric median  $\mu_{EDP|IM}$  and the associated loga-  
 160 rithmic standard deviation  $\beta_{\ln EDP|IM}$  are described by a power-law model form, which is fitted to  
 161 the discrete data points obtained from nonlinear response history analyses [i.e.,  $\mu_{EDP|IM} = a(IM)^b$ ,

162  $\beta_{\ln EDP|IM} = c(IM)^d]$ .

163 An alternative earthquake-induced loss-metric that is used in this paper is the expected annual  
 164 loss (EAL). The EAL is computed by numerically integrating the expected economic losses for a  
 165 given seismic intensity measure IM over the entire range of a seismic hazard curve at the design  
 166 site as follows,

167 
$$EAL = \int_0^{\infty} \mu_{L_T|IM} \left| \frac{d\lambda_{IM}}{dIM} \right| dIM \quad (9)$$

168 where  $\lambda_{IM}$  is the mean annual frequency of the seismic intensity IM at the site of interest. The  
 169 advantage of using EAL is that it weights all possible levels of seismic hazard by taking into  
 170 account their probability of occurrence.

171 **DESCRIPTION OF steel-frame BUILDINGS WITH SCBFs**

172 In order to assess the effect of gravity framing and the selected steel brace fragility curve on  
 173 the loss computations of steel-frame buildings with perimeter SCBFs, four archetype office steel  
 174 buildings with 2-, 3-, 6- and 12-stories are considered in this paper. The archetypes are designed as  
 175 standard office buildings (i.e., occupancy category II) according to ASCE/SEI 7-05 (ASCE 2006)  
 176 and ANSI/AISC 341-05 (AISC 2005). Details regarding their original design are discussed in  
 177 NIST (2010). In brief, the archetypes are located on a site with stiff soil denoted as Site Class  
 178 D in urban California. In order to investigate the effect of the seismic design category (SDC)  
 179 on the earthquake-induced losses in steel-frame buildings with SCBFs, two sets of archetypes are  
 180 selected. The first one is designed in Sacramento city (38.579°N, 121.493°W) for the lower bound  
 181 of SDC D (i.e., denoted as  $D_{\min}$ ). The second set of archetypes is designed in the downtown area  
 182 of Los Angeles (33.996°N, 118.162°W) for the upper bound of SDC D (i.e., denoted as  $D_{\max}$ ) in  
 183 accordance with ASCE/SEI 7-05 (ASCE 2006).

184 Steel braces in the SCBFs are designed in accordance with ANSI/AISC 341-05 (AISC 2005).  
 185 Round hollow structural sections (HSS) were used in most cases for the SCBF archetypes, except  
 186 for the 2-story archetype SCBF building designed for SDC  $D_{\max}$ . In this case, rectangular HSS  
 187 braces were used. The braces are made from ASTM A500 Grade B (i.e., nominal yield stress,



188  $F_{y,nominal}=290$  MPa for rectangular sections;  $F_{y,nominal}=315$  MPa for round sections).

189 The gusset plate connections at the steel brace ends are designed in accordance with the bal-  
190 anced design procedure as proposed by Roeder et al. (2011) that employs an elliptical clearance  
191 distance of eight times the thickness of the gusset plate ( $t_p$ ) at the corner gusset plate connections.  
192 For the design of the gusset plate connections at the mid-span of the beams, a  $6t_p$  vertical clearance  
193 distance is adopted.

194 Figure 1 illustrates a plan view and elevation of a representative 3-story archetype building  
195 with perimeter SCBFs. The use of a 2-story X-bracing configuration is adopted [see Fig. 1(b)].  
196 In order to investigate the effect of gravity framing on the earthquake-induced loss computations,  
197 the interior gravity framing system of each archetype building is explicitly designed in accordance  
198 with ANSI/AISC 360-10 (AISC 2010). The interior gravity columns are assumed to bend with  
199 respect to their weak axis as shown in Fig. 1(a).

## 200 **Site-Specific Seismic Hazard Curves**

201 The site-specific hazard curves for the two design locations discussed earlier are selected based  
202 on seismic hazard analysis. Figure 2(a) illustrates the design spectrum according to ASCE/SEI  
203 7-05 (ASCE 2006). The same figure shows the design spectral acceleration,  $S_a(T_1, 5\%)$  associated  
204 with the fundamental period,  $T_1$  of the bare model representations of the archetype buildings. From  
205 this figure, it is evident that the base shear demands for SDC  $D_{max}$  designs are much larger than  
206 those for the SDC  $D_{min}$  designs.

207 The site-specific seismic hazard curves for all the archetype buildings are shown in Fig. 2(b).  
208 These curves are obtained from the United States Geological Survey (USGS) website. The local  
209 site condition is assumed to be the National Earthquake Hazards Reduction Program (NEHRP)  
210 site class D determined based on a shear wave velocity  $v_s$  of  $259m/s$ . To better facilitate the EAL  
211 as well as the mean annual frequency of collapse,  $\lambda_c$  computations, a fourth-order polynomial is  
212 fitted to the selected hazard curves (Eads et al. 2013).

## Assumed Fragility Curves and Cost Distribution Functions

In order to reliably estimate the earthquake-induced losses in the archetype buildings their architectural layout is developed by assuming a rectangular floor area of  $2007m^2$  ( $21,600ft^2$ ). The replacement cost for an archetype building is assumed to be \$1880 (based on 2013 U.S. dollars) per square meter (i.e., \$175 per square foot). This estimation is based on the RS Means Square Foot Costs (RS Means 2013) for urban California. This is a rational cost estimate based on prior building-specific loss estimation studies (Dyanati et al. 2015).

In order to reliably quantify the earthquake-induced losses for the archetype buildings discussed herein in a probabilistic manner, it is essential to carefully define the fragility curves of their structural and nonstructural components. In an effort to retain simplicity in the loss computations, current probabilistic building-specific loss estimation methodologies (FEMA 2012) utilize univariate fragility curves (e.g., drift- or acceleration-based). However, damageable components may be very sensitive to other geometric and/or material parameters that we tend to ignore (Aslani and Miranda 2005; Lignos and Karamanci 2013). In order to quantify the effect of the used fragility curves on earthquake-induced economic losses of the archetypes discussed earlier, we utilize drift-based and dual-parameter fragility curves for steel braces as discussed in Lignos and Karamanci (2013). An example of such curves is shown in Fig. 3 for global buckling of round HSS braces. Referring to Fig. 3(a), the probability of occurrence of flexural buckling in round HSS braces at 0.5% SDR is 50%. However, depending on the global slenderness,  $KL/r$  of the respective brace (where  $K$  is the effective length factor,  $L$  is the length of the brace, and  $r$  is the radius of gyration) this value can be much larger or much smaller for the same SDR as shown in Fig. 3(b). Table 1 lists the dual-parameter fragility curves for all the considered damage states of round HSS braces.

Table 2 summarizes the repair cost associated with damage states for each damageable component identified in the archetype buildings including the respective fragility distribution curve documented in prior studies (FEMA 2012; Ramirez et al. 2012; Lignos and Karamanci 2013). The fragility parameters in Table 2 for steel columns and column splices refer to the steel-frame building performance (i.e., story-based EDP fragility curves). However, losses because of repair

240 actions in such structural components are only considered if the corresponding component under-  
241 goes inelastic deformation. The fragility curves used in this paper are primarily adopted by FEMA  
242 P-58 and other recently published literature (see Table 2). According to FEMA P-58 background  
243 documentation [see Section 1 in Deierlein and Victorsson (2008)], in modern capacity-designed  
244 steel-frame buildings it can be assumed that the framing elements (beams and columns) and their  
245 connections, as well as the brace-to-frame connections are strong enough such that the inelastic  
246 action will primarily occur in the braces through cyclic tension and compression as well as the col-  
247 umn bases (FEMA 2012). For this reason, fragility curves that describe the various damage states  
248 and the associated repair costs for beam-to-column panel zone joints are not currently available in  
249 FEMA P-58 (FEMA 2012).

## 250 **NONLINEAR BUILDING MODELS AND SIMULATION OF STRUCTURAL COLLAPSE**

251 The analytical model representation of the archetype buildings is developed within the Open  
252 System for Earthquake Engineering Simulation Platform (OPENSEES) (McKenna 1997). In order  
253 to evaluate the effect of gravity framing system on the earthquake-induced economic losses, two  
254 analytical model representations of the archetype buildings are developed. The first one considers  
255 the bare steel SCBF (i.e., bare SCBFs model, subsequently referred to as B model); the second  
256 model explicitly considers the composite floor action and the interior gravity framing system (i.e.,  
257 subsequently referred to as CG model) as discussed in Elkady and Lignos (2015).

258 The lateral load-resisting system of each building located in the east-west (E-W) loading di-  
259 rection [see Fig. 1(a)] is modeled in 2-dimensions (2-D). For illustration purposes, Fig. 4 shows  
260 the analytical model representation of a 3-story SCBF. In brief, all steel beams and columns are  
261 modeled as elastic elements with concentrated plasticity springs at their ends based on the modified  
262 Ibarra-Medina-Krawinkler (IMK) deterioration model (Ibarra et al. 2005; Lignos and Krawinkler  
263 2011). The panel zone shear distortion is explicitly modeled as discussed in Gupta and Krawinkler  
264 (1999). The steel braces in the SCBFs consist of 8 displacement-based fiber elements that are able  
265 to trace flexural buckling as well as fracture initiation because of low-cycle fatigue based on the  
266 modeling recommendations developed by Karamanci and Lignos (2014). Figure 4(c) illustrates a

267 comparison of the measured and simulated hysteretic axial force-axial displacement relation of a  
268 rectangular HSS steel brace based on the modeling recommendations discussed in Karamanci and  
269 Lignos (2014). In this figure, the experimental data were retrieved from Han et al. (2007). A non-  
270 linear out-of-plane rotational spring [see Figs. 4(a) and (b)] is placed at the ends of each brace to  
271 explicitly simulate the flexibility and flexural yielding of the gusset plates because of out-of-plane  
272 brace bending as proposed by Hsiao et al. (2013).

273 Second order effects (i.e., P-Delta effects) are explicitly considered in both B and CG models by  
274 connecting a '*leaning column*' and an '*equivalent gravity frame*', respectively, with a steel SCBF  
275 through axially rigid links. The corotational transformation is used in OPENSEES to consider the  
276 second order effects.

277 For CG models the effect of composite action on the interior gravity framing system is explic-  
278 itly captured in the CG models as discussed in Elkady and Lignos (2015). This necessitates a real-  
279 istic representation of typical shear tab beam-to-column connections used in steel-frame buildings  
280 in North America in accordance with ANSI/AISC 360-10 (AISC 2010). The shear tab beam-to-  
281 column connections that are considered in this paper consist of a single steel plate fillet welded to  
282 the supporting column with a single column of structural bolts. The distance between the beam  
283 flange to the column face is  $25mm$ . Experimental research of similar composite shear tab beam-  
284 to-column connections (Liu and Astaneh-Asl 2000) suggests that such connections can sustain up  
285 to about 40% of the fixed end moment of the steel beam with an appreciable plastic deformation  
286 capacity. Figure 4(d) illustrates a comparison of the measured and simulated moment-rotation hys-  
287 teretic relation of a composite beam as part of a single-plate shear tab beam-to-column connection.  
288 From this figure, the modeling approach used for composite shear tab beam-to-column connections  
289 reflects the experimental results.

## 290 **Structural Collapse Simulations and Associated Collapse Risk**

291 To determine the probabilistic relationship between EDPs and IM, the analytical model repre-  
292 sentations of the archetype buildings discussed earlier are subjected to a set of 44 Far-Field ground  
293 motions obtained from FEMA P695 (FEMA 2009). This set of ground motions includes twenty-

294 two component pairs of horizontal ground motion records from sites located in a distance greater  
295 than or equal to 10 *km* from the fault rupture. The magnitude  $M_w$  range of the ground motion set is  
296 from  $M_w$  6.5 to 7.6. These ground motions represent well the seismic hazard of urban California  
297 and in particular the design location of the archetype buildings. More details regarding the selected  
298 ground motion set can be found in FEMA P695 (FEMA 2009).

299 Incremental dynamic analysis (IDA) (Vamvatsikos and Cornell 2002) is used in order to trace  
300 the dynamic collapse because of sidesway instability for each archetype building. The critical  
301 EDPs of interest (i.e., peak SDRs, PFAs and RSDRs) are monitored for each ground motion over  
302 the full range of seismic intensities until the occurrence of structural collapse. Based on these  
303 recorded EDPs, the probabilistic relationship of multiple EDPs and IM is established. In this case,  
304 the  $S_a(T_1, 5\%)$  is used as an IM. However, other IMs could be used in this process as discussed in  
305 recent studies (Eads et al. 2015; Kazantzi and Vamvatsikos 2015; Kohrangi et al. 2016). Figures  
306 5(a) and (b) illustrate the IDA curves in terms of IM [i.e., the 5% damped spectral acceleration  
307 at the first mode of the building  $S_a(T_1, 5\%)$ ] versus the maximum SDRs obtained from the CG  
308 model of the 3- and 12-story steel-frame buildings with SCBFs, respectively. In these figures, the  
309 additional vertical axis at the right of each figure represents the normalized spectral acceleration  
310 with respect to the 5% damped design-basis spectral acceleration of each steel-frame building. The  
311 counted median, 16<sup>th</sup> and 84<sup>th</sup> percentiles determined based on the suite of 44 ground motions are  
312 also superimposed in Fig. 5.

313 Results from nonlinear response history analysis indicate that most of the gravity columns in  
314 the archetypes remained elastic before losses because of collapse and building demolition start to  
315 govern the total losses (i.e., up to MCE seismic intensity). For example, in the case of the 12-story  
316 CG model designed for SDC  $D_{max}$ , its gravity columns only in the upper two stories experienced  
317 inelastic deformation up to about 4% (i.e., 0.6% inelastic deformation on average) for 24 out of 32  
318 non-collapsing ground motions scaled at the MCE seismic intensity.

319 The resulting collapse capacities and record-to-record variability for each archetype are ad-  
320 justed to take into account the spectral shape effects as discussed in Haselton et al. (2011). Figure

321 6 illustrates the adjusted collapse fragility curves as computed based on the B and CG models for  
322 the SDC  $D_{\max}$  and  $D_{\min}$ . These curves describe the probability of collapse  $P_{C|IM}$  as a function of  
323 the spectral acceleration at the first mode period of the respective archetype of interest,  $S_a(T_1, 5\%)$ .  
324 From this figure, it is evident that when the composite slab action and the interior gravity framing  
325 system are considered as part of the analytical model representation, the collapse capacity of a  
326 building is normally increased, compared to that computed based on a B model regardless of the  
327 seismic design category.

328 Table 3 summarizes the median collapse capacities,  $\hat{S}_{CT}(T_1, 5\%)$  and logarithmic standard de-  
329 viations,  $\beta_{RTR}$  of the aforementioned collapse fragility curves for all the analytical model represen-  
330 tations of the archetype buildings under consideration. From this table, the composite floor system  
331 and the gravity framing typically increase the collapse capacity by 26% and 40% on average, for  
332 SDC  $D_{\max}$  and  $D_{\min}$ , respectively, compared to the collapse capacities computed based on the B  
333 model building representations.

334 The reason why the adjusted median collapse capacity and standard deviation of the 3-story  
335 archetype is nearly the same regardless of the used nonlinear building model is that the main  
336 collapse mechanisms observed based on the B and CG models are practically the same for the  
337 given set of ground motions. Figure 7 shows the main collapse mechanisms including the number  
338 of collapses per mechanism out of the 44 ground motions observed in the 3- and 6-story SCBFs  
339 based on the B and CG models. The latter is indicated as a fraction above each collapse mechanism  
340 shown in Figure 7. Referring to Figures 7(a) and 7(b), it is evident that when the gravity framing  
341 is included in the analytical model representation of the 3-story archetype there is practically no  
342 change in the number of possible collapse mechanisms. The number of collapses per mechanism is  
343 nearly identical in both cases excluding 2 ground motions in which the collapse mechanism shifted  
344 from mode III to mode II when the gravity framing was included in the nonlinear building model  
345 representation [see Figs. 7(a) and 7(b)]. In this case, the standard deviation of the collapse capacity  
346 of the 3-story archetype increases when the CG model is used compared to that computed based  
347 on the B model. Referring to Figures 7(a) and 7(b), although the total number of possible collapse

348 mechanisms of the 3-story SCBF did not change when a CG model was utilized the number of  
349 collapse mechanisms, which require fewer bracing members to fracture, was reduced.

350 Similarly, Figures 7(c) and 7(d) illustrate the possible collapse mechanisms for the 6-story  
351 archetype when the B and CG models are used, respectively. From these figures, when the gravity  
352 framing is included in the nonlinear building model, the number of possible collapse mechanisms  
353 drops from 7 to 4 in this case. From the resultant collapse mechanisms [see Figure 7(d)] it is  
354 evident that the gravity framing better distributes the peak SDRs along the height of a SCBF and  
355 prevents the concentration of inelastic deformations into single stories. In this case, the median  
356 collapse capacity of the archetype increases considerably. Furthermore, the corresponding standard  
357 deviation of the collapse fragility curve of the 6-story SCBF based on the CG model becomes  
358 smaller compared to that obtained from the B model because the total number of the collapse  
359 mechanisms becomes less [see Figures 7(c) and 7(d)].

360 Figure 8 illustrates the mean annual frequency of collapse  $\lambda_c$  of the analytical model represen-  
361 tation of the archetype buildings designed for SDC  $D_{\max}$  [see Fig. 8(a)] and  $D_{\min}$  [see Fig. 8(b)].  
362 The additional vertical axes at the right of each figure corresponds to a probability of collapse over  
363 a 50-year return period,  $P_c$  (in 50 years) by assuming a Poisson distribution. From these figures,  
364 it is evident that the estimated collapse risk of archetype buildings with SCBFs designed for SDC  
365  $D_{\max}$  and  $D_{\min}$  can be reduced by a factor of 2, on average, when incorporating the composite slab  
366 action and the gravity framing system into the analytical model representation of the respective  
367 building of interest. In this case, the 1% over 50 years collapse risk limit adopted in ASCE/SEI  
368 7-10 (ASCE 2010) is also respected regardless of the number of stories of the respective archetype  
369 steel-frame building. In most cases, such limit is not respected otherwise if a B model represen-  
370 tation is used. Therefore, the collapse risk of steel-frame buildings with SCBFs can be severally  
371 overestimated in highly seismic regions if a B model is used.

## 372 **EXPECTED LOSSES CONDITIONED ON SEISMIC INTENSITY**

373 Figure 9 shows the normalized loss vulnerability curves for the 3- and 12-story archetype build-  
374 ings designed for a SDC  $D_{\max}$  and  $D_{\min}$  based on the B model representations. In this figure, loss

375 computations are based on univariate (i.e., drift- or acceleration-based) fragility curves for each  
376 damageable component according to Table 2. Referring to Fig. 9, the expected losses (i.e., ver-  
377 tical axis) are normalized with respect to the corresponding building total replacement cost that  
378 is summarized in Table 4. The vulnerability curves illustrate the expected economic losses in an  
379 archetype building as a function of the IM,  $S_a(T_1, 5\%)$ . In Fig. 9, the expected losses conditioned  
380 on a seismic intensity are further disaggregated into losses because of structural and nonstruc-  
381 tural component repairs, losses because of demolition given that building collapse did not occur  
382 and losses because of dynamic collapse. In order to put the expected losses into perspective, the  
383 horizontal axes at the top of Fig. 9 illustrate the IM normalized with respect to the spectral ac-  
384 celeration corresponding to a design-basis earthquake (DBE) [i.e.,  $S_a(T_1, 5\%)@DBE$ ] as specified  
385 in ASCE/SEI 7-05 (ASCE 2006). These values can be obtained directly from Fig. 2(a) if the  
386 predominant period of the respective archetype building is known.

387 Referring to Fig. 9, the primary contributor to the expected losses is that from nonstructural  
388 component repairs up to the DBE seismic intensity regardless of the number of stories of the  
389 respective archetype building and the seismic design category. For the 12-story archetype building  
390 designed with SDC  $D_{max}$  [see Fig. 9(b)], losses are governed by building demolition because of  
391 excessive residual deformations along its height as well as losses because of structural collapse at  
392  $1.5 \times DBE$  seismic intensities [i.e., a maximum considered earthquake (MCE)]. In that respect, this  
393 is important particularly for mid- and high-rise steel-frame buildings designed in highly seismic  
394 regions, which are vulnerable to P-Delta effects and therefore, residual deformations may become  
395 a controlling issue. This agrees with recent research on steel special moment frames (Hwang et al.  
396 2015; Hwang and Lignos 2017). For archetype buildings designed with SDC  $D_{min}$  [see Figs. 9(c)  
397 and (d)], losses because of building demolition and structural collapse are insignificant at the MCE  
398 seismic intensity, regardless of the number of stories of the archetype building. This is in agreement  
399 with the collapse risk of the same buildings as shown in Fig. 8. The aforementioned observations  
400 are further elaborated in the subsequent paragraphs.

401 Figures 10 and 11 show the expected losses based on B and CG model representations of se-



402 lected archetype buildings at two seismic intensities of interest (i.e., DBE and MCE) at the design  
403 site of interest for SDC  $D_{\max}$  and  $D_{\min}$ , respectively. In the same figures, the influence of the used  
404 steel brace fragility curve (i.e., univariate versus bivariate) to the expected losses is also exam-  
405 ined. Referring to Figs. 10 and 11, at moderate seismic intensities (i.e., DBE seismic intensity),  
406 losses because of nonstructural component repairs seem to be indifferent to the respective analyt-  
407 ical model representation. In particular, losses because of the acceleration-sensitive nonstructural  
408 component repairs become a major contributor to the expected total losses regardless of the num-  
409 ber of stories. It is worth mentioning that the contribution of structural repairs to the total losses at  
410 the DBE seismic intensity is appreciable in most cases. This is attributed to flexural buckling of the  
411 round HSS braces. This typically occurs at SDRs in the range of 0.5%, on average (Roeder et al.  
412 2012; Lignos and Karamanci 2013). However, when the effect of steel brace global slenderness or  
413 local slenderness on the corresponding fragility curve is explicitly captured, the computed losses  
414 because of steel brace flexural buckling are reduced by 20%, on average, with respect to those  
415 computed based on drift-based steel brace fragility curves. This observation holds true regardless  
416 of the used seismic design category (see Figs. 10 and 11).

417 Referring to Fig. 10, at seismic intensities associated with low probability of occurrence earth-  
418 quakes (i.e., MCE hazard level) in highly seismic regions (i.e., SDC  $D_{\max}$ ), economic losses for  
419 mid- and high-rise steel-frame buildings are largely governed by building demolition when EDPs  
420 are based on the bare steel SCBF (i.e., B model). This is attributed to the excessive predicted  
421 residual deformations along the building height. This observation holds true regardless of the used  
422 steel brace fragility curve. It is noteworthy that when the gravity framing is explicitly considered  
423 as part of the analytical model representation of the same archetype buildings, losses because of  
424 demolition at the MCE intensity are reduced by 27 to 92% compared to those predicted from the  
425 B models. This indicates the importance of the gravity framing system in the reduction of the  
426 destabilizing (P-Delta) influence of the gravity load on steel-frame buildings with SCBFs.

427 Referring to Figs. 10(b) and (c), in mid- and high-rise archetype buildings designed with SDC  
428  $D_{\max}$ , losses because of structural collapse based on CG models are decreased significantly than

429 those computed based on B models. This observation is attributed to the fact that the drift concen-  
430 tration is not limited only to a few stories of a steel-frame building with SCBFs when the interior  
431 gravity framing system is included into the analytical model (Ji et al. 2009). Therefore, more sto-  
432 ries (i.e., more steel braces) participate into the energy dissipation during an earthquake. This also  
433 agrees well with findings from earlier studies on the contribution of the gravity framing system to  
434 the reserve capacity of steel braced frame buildings without any special detailing requirements for  
435 seismic loading (Stoakes and Fahnestock 2011; Fahnestock et al. 2014).

436 It is noteworthy that losses because of building demolition do not become a controlling issue  
437 for archetypes in relatively moderate seismicity zones (i.e., SDC  $D_{\min}$ ) (see Fig. 11). This holds  
438 true even for taller buildings that may be sensitive to P-Delta effects. In such cases, B model  
439 building representations may be used for building-specific loss assessment. This is because of the  
440 fact that very few braces fracture along the height of archetypes designed for SDC  $D_{\min}$  at the  
441 MCE intensity. For instance, looking at the simulation results from 30 out of 44 ground motions  
442 scaled at the MCE intensity that structural collapse did not occur in the CG model representation  
443 of the 12-story  $D_{\min}$  archetype, only 3 braces fractured over the frame height during 9 out of 30  
444 ground motions. In contrast, at the MCE intensity, the CG model building representation of the  
445 12-story  $D_{\max}$  archetype experienced many more brace fractures. In addition, some of its stories  
446 lost completely both braces. Therefore, plastic deformations concentrated in these stories and  
447 structural collapse occurred because of P-Delta effects.

## 448 **EXPECTED ANNUAL LOSSES**

449 In this section, the earthquake-induced losses in steel-frame buildings with SCBFs are evalu-  
450 ated based on the EAL. This loss-metric is computed by integrating the site-specific seismic hazard  
451 curves shown in Fig. 2(b) over the corresponding vulnerability curves shown in Fig. 9. The ad-  
452 vantage of using EAL as a loss-metric compared to the loss vulnerability curves discussed earlier  
453 is that EAL is calculated by considering all possible levels of seismic hazard at the design site and  
454 their probability of occurrence. Therefore, the contribution of frequent seismic events on building-  
455 specific loss estimation is more pronounced compared to loss computations at a given seismic

456 intensity.

457 Figure 12 illustrates the EALs for the 3- and 12-story archetype buildings designed for SDC  
458  $D_{\max}$  and  $D_{\min}$ . Additionally, the corresponding present value (*P.V.*) of life-cycle costs is provided  
459 in the vertical axis at the right side of each figure. The *P.V.* is simply computed by multiplying a  
460 building's EAL times its expected remaining life,  $T$  with a discount rate,  $r = 3\%$   $\left[ = EAL \times \sum_{i=1}^T (1+r)^{-i} \right]$ .  
461 In this paper, the expected remaining life of a building is assumed to be 50 years (i.e., office build-  
462 ing). Referring to Fig. 12, EALs and *P.V.* are normalized with respect to the total replacement cost  
463 of the respective building. For comparison purposes, both the B and CG model representations of  
464 the 3- and 12-story archetypes are facilitated to compute the EALs as well as the *P.V.* In order to  
465 capture the sensitivity of the EAL on the used steel brace fragility curve, the EALs are computed  
466 based on drift-based and dual-parameter steel brace fragility curves (Lignos and Karamanci 2013).  
467 In Fig. 12, EALs are further disaggregated into losses because of repairs of structural and nonstruc-  
468 tural building components (i.e., drift-sensitive and acceleration-sensitive), building demolition as  
469 well as collapse losses.

470 From Fig. 12, the EALs are practically not sensitive to the choice of the used analytical model  
471 representation nor the used steel brace fragility curve. Therefore, the simplest possible combina-  
472 tion can be utilized for building-specific loss assessment when the EAL is used as a loss-metric.  
473 Same observations hold true for the rest of the archetypes that were evaluated based on their EALs  
474 that are summarized in Table 4. From this table, the normalized EALs for archetype buildings with  
475 SCBFs typically range from 0.74 to 0.87% for SDC  $D_{\max}$  and from 0.39 to 0.65% for SDC  $D_{\min}$ .  
476 These values are consistent but slightly larger than the EALs computed for other frame buildings  
477 with conventional steel and reinforced concrete lateral load-resisting systems in North America  
478 (Ramirez et al. 2012; Hwang et al. 2015; Hwang and Lignos 2017).

479 Figure 12 illustrates that losses because of repairs in acceleration-sensitive nonstructural com-  
480 ponents dominate the total EALs regardless of the analytical model representation (i.e., B or CG  
481 model), the selected steel brace fragility curve and the used seismic design category. steel-frame  
482 buildings that utilize SCBFs are inherently stiff; therefore, absolute floor acceleration demands

483 along their height are expected to be larger than those in moment-resisting frame systems. On the  
484 other hand, losses because of repairs in drift-sensitive nonstructural components seem to be negli-  
485 gible in all cases because of the added lateral stiffness that steel braces provide compared to steel  
486 moment-resisting frame systems. Referring to Fig. 12, the contribution of SCBF structural repairs  
487 to the EALs can be appreciable for mid- and high-rise archetypes. This is attributed to flexural  
488 buckling of steel braces at fairly small SDRs (i.e., 0.5%) that can be associated to frequent and  
489 moderately frequent seismic events (i.e., 50% and 10% probability of occurrence over 50 years).

490 From Table 4 and Fig. 12, the contribution of demolition and collapse losses to the EALs is  
491 not significant. Such contributions are expected to dominate losses at seismic intensities with low  
492 probability of occurrence (i.e., extreme events). However, these events have a small weight on the  
493 EAL computations compared to that of frequent seismic events (i.e., mean annual frequency  $\lambda_{IM}$  of  
494 occurrence are  $2.1 \times 10^{-3}$  and  $4.0 \times 10^{-4}$  at given hazard levels of DBE and MCE, respectively).  
495 If the emphasis of building-specific loss estimation as well as building performance is at large  
496 deformations associated with structural collapse then it is recommended that losses conditioned on  
497 the seismic intensity of interest should be used as a loss-metric. In this case, the nonlinear building  
498 model representation should explicitly consider the gravity framing system and the composite floor  
499 action.

## 500 LIMITATIONS

501 This paper summarizes a comprehensive investigation on the effects of modeling choices as  
502 well as the used component fragility curves on the collapse risk and probabilistic economic loss  
503 assessment of steel-frame buildings with SCBFs. However, a number of limitations of the present  
504 study should be pointed out. Such limitations may provide the basis for further research. In  
505 particular:

- 506 • Even though the rotational stiffness of the column base connection may significantly af-  
507 fect the structural response [see Zareian and Kanvinde (2013)], the column bases are ide-  
508 alized as *fixed*. Experimental studies on steel column base connections [e.g., Kanvinde

509 et al. (2012) and Borzouie et al. (2014)] as well as reconnaissance reports on steel-frame  
510 buildings (Clifton et al. 2011; MacRae et al. 2015) suggest that a lower rotational stiff-  
511 ness should be used than that used in practice for “fixed” column base connections [e.g.,  
512 fixed base value of  $1.67(EI/L)_{\text{column}}$  specified in current New Zealand provisions (NZS  
513 2007)]. Despite that primary structural elements in the capacity-designed superstructure  
514 may be undergoing considerable yielding, the inherent column base flexibility may signif-  
515 icantly reduce the expected plastic deformation at the column base that ultimately affects  
516 the residual drift in the bottom story of a frame building. This issue deserves more attention  
517 and should be investigated in future studies.

- 518 ● The response of steel-frame buildings to earthquake shaking affected by the soil-foundation-  
519 structure interaction (SFSI) is not considered in this paper. This may be a critical consid-  
520 eration in cases that structural damage was not observed in steel-frame buildings (MacRae  
521 et al. 2015), This is consistent with prior analytical studies on the beneficial effect of SFSI  
522 on structural performance (i.e., reduction in peak SDRs, PFAs as well as residual defor-  
523 mations) in multi-story buildings (Givens et al. 2012; NIST 2012a; Storie et al. 2014).  
524 Therefore, the probabilistic economic losses may be overstated when ignoring the SFSI ef-  
525 fect into the analytical model representation of the respective building. This issue deserves  
526 more attention in future research studies.
- 527 ● Losses because of repair or replacement of acceleration-sensitive nonstructural components  
528 herein are derived based on fragility curves with fairly low median PFAs at each damage  
529 state as suggested in FEMA P-58 (FEMA 2012). However, this may not be consistent  
530 with damage observations in steel-frame buildings from the 2010/2011 Christchurch earth-  
531 quakes (Clifton et al. 2011). In particular, no damage was observed to either the suspended  
532 ceilings or the sprinkler (i.e., components sensitive to PFAs) installed in steel buildings  
533 subjected to a PGA of 0.55 g and PFAs of 0.55–0.7 g. Therefore, loss estimation of non-  
534 structural acceleration-sensitive components may be conservative to some extent.
- 535 ● The earthquake-induced economic losses presented herein are based on fragility curves for

536 building components available in recently published literature (FEMA 2012; Ramirez et al.  
537 2012; Lignos and Karamanci 2013). For instance, specific components such as elevator re-  
538 pairs may be more influenced by residual drifts instead of PGA, as the lift shaft guiderails  
539 may require realignment in the case of permanent deformations along the height of a build-  
540 ing (Clifton et al. 2011). Therefore refined component fragility curves should be developed  
541 when new experimental data become available.

## 542 CONCLUSIONS

543 This paper assessed the effect of analytical modeling assumptions on the collapse risk and  
544 the earthquake-induced economic losses for typical archetype steel-frame buildings with special  
545 concentrically braced frames (SCBFs) ranging from 2- to 12-stories. This was achieved through  
546 the development of analytical model representations of the bare SCBF only (namely as B model)  
547 as well as models that captured explicitly the effect of the gravity framing and the composite floor  
548 action (namely as CG model) on the steel-frame building's structural response. Typical archetypes  
549 were designed in two different seismic zones in urban California; the first one represented the  
550 lower bound of the Seismic Design Category D (referred to as SDC  $D_{\min}$ ); and the second one  
551 represented the upper bound of the Seismic Design Category D (referred to as SDC  $D_{\max}$ ). A  
552 comprehensive probabilistic loss estimation methodology was used (Ramirez and Miranda 2012)  
553 and refined that rigorously integrates multiple engineering demand parameters (EDPs) for a wide  
554 range of seismic intensities representing frequent seismic events as well as earthquakes with low  
555 probability of occurrence. The earthquake-induced economic losses were evaluated in terms of  
556 expected losses conditioned on a seismic intensity (i.e., loss vulnerability curves) and the expected  
557 annual losses (EALs). The effect of the used steel brace fragility curve on the loss computations  
558 was also quantified. The main findings are summarized as follows:

- 559 1. Damage in acceleration-sensitive nonstructural components seem to govern the total losses  
560 in steel-frame buildings with SCBFs at frequent and design basis seismic events. The  
561 magnitude of such losses is not sensitive to the selected analytical model representation,

562 the number of stories of the respective archetype building and the used loss-metric.

- 563 2. Losses because of steel brace damage seem to be appreciable at frequent and design-basis  
564 earthquakes. This is because of the fact that steel brace flexural buckling may occur at  
565 fairly small drift ratios (i.e., 0.5% on average). In this case, the choice of the used steel  
566 brace fragility curve affects the loss computations. In particular, drift-based fragility curves  
567 commonly used in the earthquake engineering practice tend to overestimate repairs of steel  
568 brace components by approximately 20% compared to dual-parameter steel brace fragility  
569 curves. The latter captures the effect of brace geometry (i.e., global and local slenderness)  
570 on loss computations for a given story drift ratio.
- 571 3. If losses because of demolition and collapse are of fundamental concern, they should be  
572 evaluated conditioned on the seismic intensity of interest. In this case, the choice of the  
573 analytical model representation of the archetype building becomes significant especially  
574 for steel-frame buildings designed in highly seismic regions (i.e., SDC  $D_{\max}$ ). In particular,  
575 nonlinear building models that explicitly capture the destabilizing effects of the gravity  
576 framing (i.e., CG models) should be used. Else, losses because of demolition are largely  
577 overestimated because of drift concentrations in few stories of a steel SCBF that in reality  
578 are not as pronounced as B models predict.
- 579 4. steel-frame buildings with perimeter SCBFs designed for a SDC  $D_{\max}$  achieved a probabilit-  
580 ity of collapse in 50 years that satisfied the 1% limit specified by ASCE/SEI 7-10 (ASCE  
581 2010) only when the contribution of the composite slab action and the gravity framing was  
582 considered as part of the analytical model building representation. Models that consider the  
583 bare frame only seem to largely overestimate the collapse risk of steel-frame buildings with  
584 SCBFs in highly seismic regions. This is not a controlling issue for steel SCBFs designed  
585 for a SDC  $D_{\min}$ .
- 586 5. The EAL is a more representative metric to evaluate losses in steel-frame buildings with  
587 SCBFs for seismic events with moderate to high probability of occurrence (i.e., more fre-  
588 quently occurring seismic events) compared to loss-metrics that are conditioned on a single

589 seismic intensity. The reason is that more frequent seismic events are better weighted in  
590 the EAL computations through the integration of the loss vulnerability curve of a building  
591 over the design site-specific hazard curve. In this case, detailed modeling of the respective  
592 building of interest does not seem to be critical for the cases considered in this paper.

- 593 6. The normalized EALs for low- to high-rise steel-frame buildings with SCBFs range from  
594 0.74 to 0.87% for SDC  $D_{\max}$  and from 0.39 to 0.65% for SDC  $D_{\min}$ . These values seem  
595 to be insensitive to the choice of the analytical modeling representation of the respective  
596 archetype and the choice of the steel brace fragility curve. In addition, the above EAL  
597 range is consistent but slightly larger than the corresponding values for other conventional  
598 steel and reinforced concrete frame buildings designed in seismic regions.

## 599 **ACKNOWLEDGMENTS**

600 This study is based on work supported by the Fonds de recherché du Québec - Nature et tech-  
601 nologies, Projet de Recherché en Equipe, Award No. FQRNT 2013-PR-167747. Financial support  
602 was also provided by the Swiss Federal Institute of Technology in Lausanne (EPFL). The financial  
603 support is gratefully acknowledged. Any opinions, findings, and conclusions or recommendations  
604 expressed in this paper are those of the authors and do not necessarily reflect the views of the  
605 sponsors.



## REFERENCES

- AISC (2005). "Seismic provisions for structural steel buildings." *ANSI/AISC 341-05*, American Institute of Steel Construction, Chicago, IL.
- AISC (2010). "Specification for structural steel buildings." *ANSI/AISC 360-10*, American Institute of Steel Construction, Chicago, IL.
- Aitchison, J. and Brown, J. A. C. (1957). *The lognormal distribution with special reference to its uses in Economics*. Cambridge University Press, Cambridge.
- ASCE (2006). "Minimum design loads for buildings and other structures." *ASCE/SEI 7-05*, American Society of Civil Engineers, Reston, VA.
- ASCE (2010). "Minimum design loads for buildings and other structures." *ASCE/SEI 7-10*, American Society of Civil Engineers, Reston, VA.
- Aslani, H. and Miranda, E. (2005). "Fragility assessment of slab-column connections in existing non-ductile reinforced concrete buildings." *Journal of Earthquake Engineering*, 9(6), 777–804.
- Baradaran Shoraka, M., Yang, T. Y., and Elwood, K. J. (2013). "Seismic loss estimation of non-ductile reinforced concrete buildings." *Earthquake Engineering & Structural Dynamics*, 42(2), 297–310.
- Borzouie, J., MacRae, G. A., Chase, J. G., and Clifton, G. C. (2014). "Experimental studies on cyclic behaviour of steel base plate connections considering anchor bolts post tensioning." *Proceedings of 2014 New Zealand Society for Earthquake Engineering Annual Conference*, Auckland, New Zealand.
- Chopra, A. K. (2011). *Dynamics of structures: Theory and applications to earthquake engineering*. Prentice Hall, Upper Saddle River, NJ, 4th edition.
- Clifton, G. C., Bruneau, M., MacRae, G., Leon, R., and Fussell, A. (2011). "Steel structures damage from the Christchurch earthquake series of 2010 and 2011." *Bulletin of the New Zealand Society for Earthquake Engineering*, 44(4), 297–318.
- Cornell, C. A. and Krawinkler, H. (2000). "Progress and challenges in seismic performance assessment." *PEER Center News*, 3(2), 1–3.

633 Deierlein, G. G. and Victorsson, V. (2008). “Fragility curves for components of steel SMF sys-  
634 tems.” *Background document of FEMA P-58/BD-3.8.3*, prepared by the Applied Technology  
635 Council for the Federal Emergency Management Agency, Washington, DC.

636 Dyanati, M., Huang, Q., and Roke, D. (2015). “Life cycle cost-benefit evaluation of self-centering  
637 and conventional concentrically braced frames.” *Proceedings of 12th International Conference*  
638 *on Applications of Statistics and Probability in Civil Engineering, ICASP12*, Vancouver, BC,  
639 Canada.

640 Eads, L., Miranda, E., Krawinkler, H., and Lignos, D. G. (2013). “An efficient method for esti-  
641 mating the collapse risk of structures in seismic regions.” *Earthquake Engineering & Structural*  
642 *Dynamics*, 42(1), 25–41.

643 Eads, L., Miranda, E., and Lignos, D. G. (2015). “Average spectral acceleration as an intensity  
644 measure for collapse risk assessment.” *Earthquake Engineering & Structural Dynamics*, 44(12),  
645 2057–2073.

646 Elkady, A. and Lignos, D. G. (2015). “Effect of gravity framing on the overstrength and collapse  
647 capacity of steel frame buildings with perimeter special moment frames.” *Earthquake Engineer-*  
648 *ing & Structural Dynamics*, 44(8), 1289–1307.

649 Fahnestock, L. A., Hines, E. M., Tremblay, R., Bradley, C., Nelson, J., Beland, T., Davaran, A.,  
650 and Sizemore, J. (2014). “Reserve capacity and implications for seismic collapse prevention  
651 for low-ductility braced frames in moderate seismic regions.” *Proceedings of 10th U.S. National*  
652 *Conference on Earthquake Engineering: Frontiers of Earthquake Engineering*, Anchorage, AK.

653 FEMA (2009). “Quantification of building seismic performance factors.” *Report No. FEMA-P695*,  
654 Federal Emergency Management Agency, Washington, DC.

655 FEMA (2012). “Seismic performance assessment of buildings, volume 1-methodology.” *Report*  
656 *No. FEMA P-58-1*, prepared by the Applied Technology Council for the Federal Emergency  
657 Management Agency, Washington, DC.

658 Flores, F. X., Charney, F. A., and Lopez-Garcia, D. (2014). “Influence of the gravity framing  
659 system on the collapse performance of special steel moment frames.” *Journal of Constructional*

660 *Steel Research*, 101, 351–362.

661 Flores, F. X., Charney, F. A., and Lopez-Garcia, D. (2016). “The influence of gravity column  
662 continuity on the seismic performance of special steel moment frame structures.” *Journal of*  
663 *Constructional Steel Research*, 118, 217–230.

664 Givens, M. J., Stewart, J. P., Haselton, C. B., and Mazzoni, S. (2012). “Assessment of soil-structure  
665 interaction modeling strategies for response history analysis of buildings.” *Proceedings of the*  
666 *15th World Conference on Earthquake Engineering (15WCEE)*, Lisbon, Portugal.

667 Gupta, A. and Krawinkler, H. (1999). “Seismic demands for the performance evaluation of steel  
668 moment resisting frame structures.” *Blume Center Technical Report No. 132*, The John A. Blume  
669 Earthquake Engineering Center, Stanford University, Stanford, CA.

670 Han, S.-W., Kim, W. T., and Foutch, D. A. (2007). “Seismic behavior of HSS bracing members  
671 according to width-thickness ratio under symmetric cyclic loading.” *Journal of Structural Engi-*  
672 *neering*, 133(2), 264–273.

673 Haselton, C. B., Baker, J. W., Liel, A. B., and Deierlein, G. G. (2011). “Accounting for ground-  
674 motion spectral shape characteristics in structural collapse assessment through an adjustment for  
675 epsilon.” *Journal of Structural Engineering*, 137(3), 332–344.

676 Hsiao, P.-C., Lehman, D. E., and Roeder, C. W. (2013). “A model to simulate special concentrically  
677 braced frames beyond brace fracture.” *Earthquake Engineering & Structural Dynamics*, 42(2),  
678 183–200.

679 Hwang, S.-H., Elkady, A., Bardaweel, S. A., and Lignos, D. G. (2015). “Earthquake loss assess-  
680 ment of steel frame buildings designed in highly seismic regions.” *Proceedings of 5th ECCO-*  
681 *MAS Thematic Conference on Computational Methods in Structural Dynamics and Earthquake*  
682 *Engineering*, Crete Island, Greece, 1496–1512.

683 Hwang, S.-H. and Lignos, D. G. (2017). “Earthquake-induced loss assessment of steel frame build-  
684 ings with special moment frames designed in highly seismic regions.” *Earthquake Engineering*  
685 *& Structural Dynamics*, DOI:10.1002/eqe.2898, in press.

686 Ibarra, L. F., Medina, R. A., and Krawinkler, H. (2005). “Hysteretic models that incorporate

687 strength and stiffness deterioration.” *Earthquake Engineering & Structural Dynamics*, 34(12),  
688 1489–1511.

689 Ji, X., Kato, M., Wang, T., Hitaka, T., and Nakashima, M. (2009). “Effect of gravity columns on  
690 mitigation of drift concentration for braced frames.” *Journal of Constructional Steel Research*,  
691 65(12), 2148–2156.

692 Kanvinde, A. M., Grilli, D. A., and Zareian, F. (2012). “Rotational stiffness of exposed col-  
693 umn base connections: Experiments and analytical models.” *Journal of Structural Engineering*,  
694 138(5), 549–560.

695 Karamanci, E. and Lignos, D. G. (2014). “Computational approach for collapse assessment of  
696 concentrically braced frames in seismic regions.” *Journal of Structural Engineering*, 140(8),  
697 A4014019.

698 Kazantzi, A. K. and Vamvatsikos, D. (2015). “Intensity measure selection for vulnerability studies  
699 of building classes.” *Earthquake Engineering & Structural Dynamics*, 44(15), 2677–2694.

700 Kohrangi, M., Bazzurro, P., and Vamvatsikos, D. (2016). “Vector and scalar IMs in structural  
701 response estimation, part II: Building demand assessment.” *Earthquake Spectra*, 32(3), 1525–  
702 1543.

703 Li, Y. and van de Lindt, J. W. (2012). “Loss-based formulation for multiple hazards with applica-  
704 tion to residential buildings.” *Engineering Structures*, 38, 123–133.

705 Liel, A. B. and Deierlein, G. G. (2013). “Cost-benefit evaluation of seismic risk mitigation alter-  
706 natives for older concrete frame buildings.” *Earthquake Spectra*, 29(4), 1391–1411.

707 Lignos, D. G. and Karamanci, E. (2013). “Drift-based and dual-parameter fragility curves for  
708 concentrically braced frames in seismic regions.” *Journal of Constructional Steel Research*, 90,  
709 209–220.

710 Lignos, D. G. and Krawinkler, H. (2011). “Deterioration modeling of steel components in support  
711 of collapse prediction of steel moment frames under earthquake loading.” *Journal of Structural  
712 Engineering*, 137(11), 1291–1302.

713 Liu, J. and Astaneh-Asl, A. (2000). “Cyclic testing of simple connections including effects of slab.”

714 *Journal of Structural Engineering*, 126(1), 32–39.

715 MacRae, G., Clifton, G. C., Bruneau, M., Kanvinde, A., and Gardiner, S. (2015). “Lessons from  
716 steel structures in Christchurch earthquakes.” *Proceedings of 8th International Conference on  
717 Behavior of Steel Structures in Seismic Areas (STESSA)*, Shanghai, China, 1474–1481.

718 MacRae, G. A., Kimura, Y., and Roeder, C. (2004). “Effect of column stiffness on braced frame  
719 seismic behavior.” *Journal of Structural Engineering*, 130(3), 381–391.

720 *MATLAB Version 8.5.0 (R2015a)* (2015). The Math Works, Inc., Natick, MA.

721 McKenna, F. T. (1997). “Object oriented finite element programming frameworks for analysis, al-  
722 gorithms and parallel computings.” Ph.D. thesis, University of California at Berkeley, Berkeley,  
723 CA.

724 Mitrani-Reiser, J. (2007). “An ounce of prevention: probabilistic loss estimation for performance-  
725 based earthquake engineering.” Ph.D. thesis, California Institute of Technology, Pasadena, CA.

726 NIST (2010). “Evaluation of the FEMA P-695 methodology for quantification of building seismic  
727 performance factors.” *Report No. NIST GCR 10-917-8*, prepared by the NEHRP Consultants  
728 Joint Venture for the National Institute of Standards and Technology, Gaithersburg, MD.

729 NIST (2012a). “Soil-structure interaction for building structures.” *Report No. NIST GCR 12-917-  
730 21*, prepared by the NEHRP Consultants Joint Venture for the National Institute of Standards  
731 and Technology, Gaithersburg, MD.

732 NIST (2012b). “Tentative framework for development of advanced seismic design criteria for new  
733 buildings.” *Report No. NIST GCR 12-917-20*, prepared by the NEHRP Consultants Joint Venture  
734 for the National Institute of Standards and Technology, Gaithersburg, MD.

735 NZS (2007). “Steel structures standard, incorporating amendments No. 1 and No. 2.” *NZS 3404*,  
736 Standards New Zealand, Wellington, New Zealand.

737 Pei, S. and van de Lindt, J. W. (2009). “Methodology for earthquake-induced loss estimation: An  
738 application to woodframe buildings.” *Structural Safety*, 31(1), 31–42.

739 Porter, K. A., Kiremidjian, A. S., and LeGrue, J. S. (2001). “Assembly-based vulnerability of  
740 buildings and its use in performance evaluation.” *Earthquake Spectra*, 17(2), 291–312.

741 Porter, K. A., Scawthorn, C. R., and Beck, J. L. (2006). “Cost-effectiveness of stronger woodframe  
742 buildings.” *Earthquake Spectra*, 22(1), 239–266.

743 Ramirez, C. M., Liel, A. B., Mitrani-Reiser, J., Haselton, C. B., Spear, A. D., Steiner, J., Deierlein,  
744 G. G., and Miranda, E. (2012). “Expected earthquake damage and repair costs in reinforced  
745 concrete frame buildings.” *Earthquake Engineering & Structural Dynamics*, 41(11), 1455–1475.

746 Ramirez, C. M. and Miranda, E. (2012). “Significance of residual drifts in building earthquake loss  
747 estimation.” *Earthquake Engineering & Structural Dynamics*, 41(11), 1477–1493.

748 Ray-Chaudhuri, S. and Hutchinson, T. C. (2011). “Effect of nonlinearity of frame buildings on  
749 peak horizontal floor acceleration.” *Journal of Earthquake Engineering*, 15(1), 124–142.

750 Rodriguez, M. E., Restrepo, J. I., and Carr, A. J. (2002). “Earthquake-induced floor horizontal  
751 accelerations in buildings.” *Earthquake Engineering & Structural Dynamics*, 31(3), 693–718.

752 Roeder, C. W., Lumpkin, E. J., and Lehman, D. E. (2011). “A balanced design procedure for  
753 special concentrically braced frame connections.” *Journal of Constructional Steel Research*,  
754 67(11), 1760–1772.

755 Roeder, C. W., Lumpkin, E. J., and Lehman, D. E. (2012). “Seismic performance assessment of  
756 concentrically braced steel frames.” *Earthquake Spectra*, 28(2), 709–727.

757 RS Means (2013). *RS Means Square Foot Costs*. RS Means Corp., Kingston, MA. USA.

758 Song, R., Li, Y., and van de Lindt, J. W. (2016). “Loss estimation of steel buildings to earthquake  
759 mainshockaftershock sequences.” *Structural Safety*, 61, 1–11.

760 Stoakes, C. D. and Fahnestock, L. A. (2011). “Cyclic flexural testing of concentrically braced  
761 frame beam-column connections.” *Journal of Structural Engineering*, 137(7), 739–747.

762 Storie, L. B., Pender, M. J., Clifton, G. C., and Wotherspoon, L. M. (2014). “Soil-foundation-  
763 structure interaction for buildings on shallow foundations in the Christchurch earthquake.” *Pro-  
764 ceedings of tenth U.S. National Conference on Earthquake Engineering Frontiers of Earthquake  
765 Engineering (10NCEE)*, Anchorage, AK.

766 Tremblay, R. (2002). “Inelastic seismic response of steel bracing members.” *Journal of Construc-  
767 tional Steel Research*, 58(5-8), 665–701.

- 768 Tremblay, R., Filiatrault, A., Bruneau, M., Nakashima, M., Prion, H. G. L., and DeVall, R. (1996).  
769 “Seismic design of steel buildings: lessons from the 1995 Hyogo-ken Nanbu earthquake.” *Can-*  
770 *adian Journal of Civil Engineering*, 23(3), 727–756.
- 771 Tremblay, R., Filiatrault, A., Timler, P., and Bruneau, M. (1995). “Performance of steel structures  
772 during the 1994 Northridge earthquake.” *Canadian Journal of Civil Engineering*, 22(2), 338–  
773 360.
- 774 Vamvatsikos, D. and Cornell, C. A. (2002). “Incremental dynamic analysis.” *Earthquake Engi-*  
775 *neering & Structural Dynamics*, 31(3), 491–514.
- 776 Zareian, F. and Kanvinde, A. (2013). “Effect of column-base flexibility on the seismic response  
777 and safety of steel moment-resisting frames.” *Earthquake Spectra*, 29(4), 1537–1559.

778  
779  
780  
781  
782  
783  
784  
785

## List of Tables

1	Dual-parameter fragility distribution functions for steel braces (Lignos and Karamanci 2013) . . . . .	33
2	Fragility and cost estimates for steel-frame buildings with perimeter SCBFs . . . .	34
3	Median and logarithmic standard deviation of collapse fragility curves for all the analytical model representations of the archetype steel buildings with SCBFs . . .	37
4	Normalized EALs for archetype buildings with SCBFs based on drift-based steel brace fragility curves . . . . .	38



**TABLE 1 Dual-parameter fragility distribution functions for steel braces (Lignos and Karamanci 2013)**

Assembly description	Damage state <sup>a</sup>	Fragility parameters					
		$\mu_{SDR}$ (%)	$\beta_{lnSDR}$	$\mu_{KL/r}$	$\beta_{lnKL/r}$	$\mu_{(D/t)/\lambda_{hd}^b}$	$\beta_{ln(D/t)/\lambda_{hd}^b}$
Round HSS Braces	DS1	0.41	0.51	63.6	0.46	0.97	0.47
	DS2	0.96	0.45	66.1	0.45	1.02	0.42
	DS3	2.75	0.51	68.9	0.40	1.11	0.33

<sup>a</sup> DS1 = global buckling; DS2 = local buckling; and DS3 = brace fracture.

<sup>b</sup>  $\lambda_{hd}$  = the corresponding seismic compactness limit specified in AISC (2010).

**TABLE 2 Fragility and cost estimates for steel-frame buildings with perimeter SCBFs**

Assembly description	Damage state <sup>a</sup>	Unit	Fragility parameters			Repair cost parameters
			EDP <sup>b</sup>	$x_m^c$	$\beta^d$	$x_m^c$ (\$)
Columns base (W < 223kg/m) (FEMA 2012)	Crack initiation	EA	SDR	0.04	0.40	19224
	Crack propagation			0.07	0.40	27263
	Fracture			0.10	0.40	32423
Columns base (223kg/m < W ≤ 446kg/m) (FEMA 2012)	Crack initiation	EA	SDR	0.04	0.40	20082
	Crack propagation			0.07	0.40	29395
	Fracture			0.10	0.40	36657
Columns base (W > 446kg/m) (FEMA 2012)	Crack initiation	EA	SDR	0.04	0.40	21363
	Crack propagation			0.07	0.40	32567
	Fracture			0.10	0.40	41890
Column splices (W < 223kg/m) (FEMA 2012)	Crack initiation	EA	SDR	0.04	0.40	9446
	Crack propagation			0.07	0.40	11246
	Fracture			0.10	0.40	38473
Column splices (223kg/m < W ≤ 446kg/m) (FEMA 2012)	Crack initiation	EA	SDR	0.04	0.40	10246
	Crack propagation			0.07	0.40	13012
	Fracture			0.10	0.40	42533
Column splices (W > 446kg/m) (FEMA 2012)	Crack initiation	EA	SDR	0.04	0.40	11446
	Crack propagation			0.07	0.40	14812
	Fracture			0.10	0.40	47594
Column (≤ W27) (FEMA 2012)	LB	EA	SDR	0.03	0.30	16033
	LTB			0.04	0.30	25933
	Fracture			0.05	0.30	25933
Column (≥ W30) (FEMA 2012)	LB	EA	SDR	0.03	0.30	17033
	LTB			0.04	0.30	28433
	Fracture			0.05	0.30	28433
Rectangular HSS (Brace weight < 60kg/m) (Lignos and Karamanci 2013)	GB	EA	SDR	0.40	0.43	29983
	LB			1.02	0.44	37014
	Brace Fracture			1.60	0.48	36480
Rectangular HSS (61kg/m < Brace weight < 147kg/m) (Lignos and Karamanci 2013)	GB	EA	SDR	0.40	0.43	29983
	LB			1.02	0.44	47115
	Brace Fracture			1.60	0.48	47882

**TABLE 2 Fragility and cost estimates for steel-frame buildings with perimeter SCBFs (continued)**

Assembly description	Damage state <sup>a</sup>	Unit	Fragility parameters			Repair cost parameters
			EDP <sup>b</sup>	$x_m^c$	$\beta^d$	$x_m^c$ (\$)
Round HSS (Brace weight < 60kg/m) (Lignos and Karamanci 2013)	GB	EA	SDR	0.41	0.51	29983
	LB			0.96	0.45	37014
	Brace Fracture			2.75	0.51	36480
Round HSS (61kg/m < Brace weight < 147kg/m) (Lignos and Karamanci 2013)	GB	EA	SDR	0.41	0.51	29983
	LB			0.96	0.45	47115
	Brace Fracture			2.75	0.51	47882
Moment connections (one-sided, ≤ W27) (FEMA 2012)	LB	EA	SDR	0.03	0.30	16033
	LTB			0.04	0.30	25933
	Fracture			0.05	0.30	25933
Moment connections(one-sided, ≥ W30) (FEMA 2012)	LB	EA	SDR	0.03	0.30	17033
	LTB			0.04	0.30	28433
	Fracture			0.05	0.30	28433
Moment connections (two-sided, ≤ W27) (FEMA 2012)	LB	EA	SDR	0.03	0.30	30400
	LTB			0.04	0.30	47000
	Fracture			0.05	0.30	47000
Moment connections (two-sided, ≥ W30) (FEMA 2012)	LB	EA	SDR	0.03	0.30	30400
	LTB			0.04	0.30	52399
	Fracture			0.05	0.30	52399
Shear tab connections (FEMA 2012)	Yielding	EA	SDR	0.04	0.40	12107
	Partial tearing			0.08	0.40	12357
	Complete separation			0.11	0.40	12307
Corrugated slab (90mm steel; 100mm overlay) (Hwang et al. 2015)	Crack initiations	m <sup>2</sup>	SDR	0.00375	0.13	180
	Crushing near column			0.01	0.22	330
	Shear stud fracture			0.05	0.35	570
Drywall partition (Ramirez et al. 2012)	Visible	6m <sup>2</sup>	SDR	0.0039	0.17	90
	Significant			0.0085	0.23	530
Drywall finish (Ramirez et al. 2012)	Visible	6m <sup>2</sup>	SDR	0.0039	0.17	90
	Significant			0.0085	0.23	250
Exterior glazing (Ramirez et al. 2012)	Crack	pane	SDR	0.04	0.36	440
	Fallout			0.046	0.33	440
Suspended ceiling (A > 232m <sup>2</sup> ) (FEMA 2012)	5% tiles dislodge	232m <sup>2</sup>	PFA(g)	0.35	0.40	3542
	30% tiles dislodge			0.55	0.40	29337
	Collapse			0.80	0.40	55200

**TABLE 2 Fragility and cost estimates for steel-frame buildings with perimeter SCBFs (continued)**

Assembly description	Damage state <sup>a</sup>	Unit	Fragility parameters			Repair cost parameters
			EDP <sup>b</sup>	$x_m^c$	$\beta^d$	$x_m^c$ (\$)
Automatic sprinklers (Ramirez et al. 2012)	Fracture	3.66m	PFA( g)	0.32	1.40	900
Elevator (FEMA 2012)	Failure	EA	PGA( g)	0.50	0.28	868

<sup>a</sup>GB=Global buckling, LB=local buckling, LTB=lateral-torsional buckling.

<sup>b</sup>SDR=story drift ratio, PFA=peak floor acceleration ( g), PGA=peak ground acceleration ( g).

<sup>c</sup>  $x_m$ =median value of assembly fragility curve.

<sup>d</sup>  $\beta$ =lognormal standard deviation.

**TABLE 3 Median and logarithmic standard deviation of collapse fragility curves for all the analytical model representations of the archetype steel buildings with SCBFs**

No. of stories	$\hat{S}_{CT}(T_1, 5\%) / g$				$\beta_{RTR}$			
	SDC D <sub>max</sub>		SDC D <sub>min</sub>		SDC D <sub>max</sub>		SDC D <sub>min</sub>	
	<i>B</i>	<i>CG</i>	<i>B</i>	<i>CG</i>	<i>B</i>	<i>CG</i>	<i>B</i>	<i>CG</i>
2	2.96	3.75	1.30	1.90	0.48	0.48	0.56	0.54
3	4.22	4.31	1.76	1.90	0.50	0.54	0.56	0.61
6	2.51	3.09	1.34	1.73	0.59	0.48	0.60	0.58
12	1.11	1.68	0.71	1.23	0.73	0.63	0.50	0.53

**TABLE 4 Normalized EALs for archetype buildings with SCBFs based on drift-based steel brace fragility curves**

Building model		Replacement cost (millions U.S. dollars)	EAL (%)					Total losses
			nonstructural losses		Structural losses	Demolition losses	Collapse losses	
			Acc	Drift				
<b>SDC D<sub>max</sub></b>								
2	<i>B</i>	7.56	0.623	0.020	0.061	0.092	0.020	0.816
	<i>CG</i>		0.690	0.022	0.068	0.012	0.009	0.801
3	<i>B</i>	11.34	0.648	0.027	0.049	0.011	0.004	0.738
	<i>CG</i>		0.707	0.025	0.047	0.008	0.005	0.792
6	<i>B</i>	22.68	0.663	0.049	0.071	0.034	0.015	0.832
	<i>CG</i>		0.666	0.043	0.061	0.013	0.005	0.788
12	<i>B</i>	45.36	0.562	0.063	0.159	0.045	0.043	0.872
	<i>CG</i>		0.623	0.044	0.113	0.006	0.015	0.801
<b>SDC D<sub>min</sub></b>								
2	<i>B</i>	7.56	0.315	0.012	0.040	0.005	0.020	0.392
	<i>CG</i>		0.395	0.013	0.037	0.000	0.005	0.450
3	<i>B</i>	11.34	0.521	0.015	0.036	0.001	0.003	0.577
	<i>CG</i>		0.594	0.015	0.035	0.000	0.004	0.647
6	<i>B</i>	22.68	0.334	0.035	0.059	0.002	0.002	0.432
	<i>CG</i>		0.419	0.029	0.051	0.000	0.001	0.501
12	<i>B</i>	45.36	0.395	0.044	0.132	0.005	0.001	0.577
	<i>CG</i>		0.435	0.029	0.090	0.001	0.000	0.556

Note that all values in the table are expressed as a percentage of the total replacement cost of the respective building

**List of Figures**

786

787 1 Archetype steel-frame buildings with perimeter SCBFs: (a) typical plan view; and

788 (b) elevation view of the 3-story SCBF . . . . . 41

789 2 Design spectrum and site-specific seismic hazard curves for bare model represen-

790 tations of archetype buildings with SCBFs . . . . . 42

791 3 Example of fragility curves for damage state of global buckling for round HSS

792 braces: (a) univariate fragility curve; and (b) dual-parameter (global slenderness

793  $KL/r$ ) fragility curves [adopted from Lignos and Karamanci (2013)] . . . . . 43

794 4 Analytical model representation of steel-frame buildings with SCBFs: (a) 2-D an-

795 alytical model including the gravity framing (CG model); (b) description of the

796 steel brace component model; (c) axial force-deformation relation for rectangular

797 HSS brace section [data from Han et al. (2007)]; and (d) moment-chord rotation

798 relation for composite beam in single-plate shear tab connections [data from Liu

799 and Astaneh-Asl (2000)] . . . . . 44

800 5 IDA curves for the 3- and 12-story steel-frame buildings with perimeter SCBFs

801 (CG models) . . . . . 45

802 6 Collapse fragility curves for steel-frame buildings with perimeter SCBFs with/without

803 gravity framing system . . . . . 46

804 7 Collapse mechanisms for the 3- and 6-story archetypes based on B and CG models 47

805 8 Mean annual frequency of collapse  $\lambda_c$  and the corresponding collapse probability

806 over 50 years  $P_c$  (in 50 years) for the analytical model type of archetype buildings

807 with perimeter SCBFs . . . . . 48

808 9 Normalized loss vulnerability curves for steel-frame buildings with perimeter SCBFs

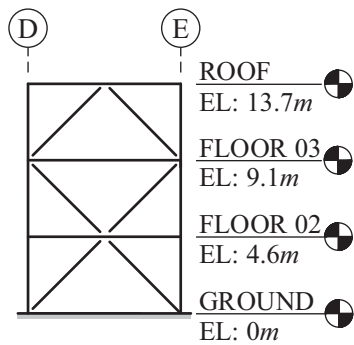
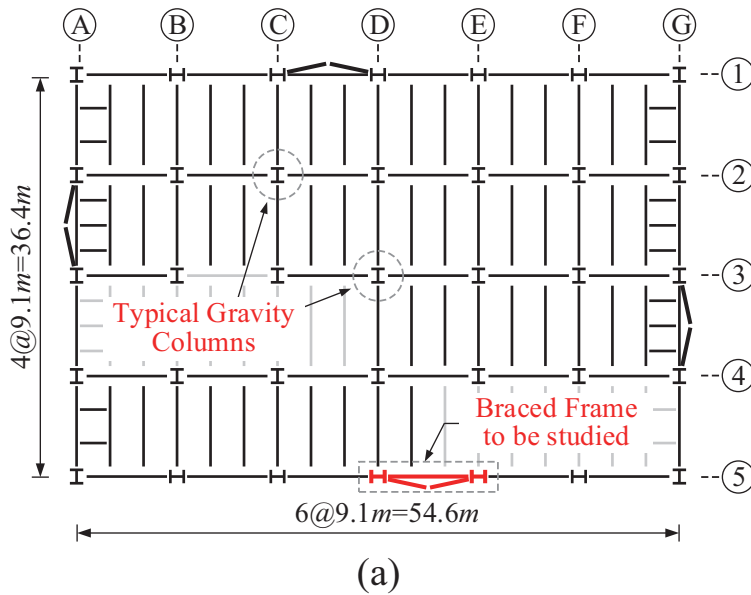
809 designed for SDC  $D_{max}$  and  $D_{min}$  conditioned on seismic intensity . . . . . 49

810 10 Normalized expected losses of steel-frame buildings with perimeter SCBFs de-

811 signed for SDC  $D_{max}$  conditioned on selected seismic intensities . . . . . 50

812 11 Normalized expected losses of the 12-story steel-frame building with perimeter  
813 SCBFs designed for SDC  $D_{min}$  conditioned on selected seismic intensities . . . . . 51  
814 12 Normalized expected annual losses and present values for steel-frame buildings  
815 with SCBFs . . . . . 52





**Note:**

**Gravity Loads**

1. Roof Loading
  - Dead = 3.21 kPa
  - Live = 0.96 kPa
2. Floor Loading
  - Dead = 4.07 kPa
  - Live = 2.39 kPa

**Seismic Design Parameters**

Occupancy Category II  
(office)

Importance Factor = 1.0

$R = 6, C_d = 6, \Omega_0 = 2.0$

Seismic Design Category *D*

1.  $D_{max}$

$S_{DS} = 1.4g, S_{D1} = 0.7g$

$F_a = 1.0, F_v = 1.5$

Los Angeles, California

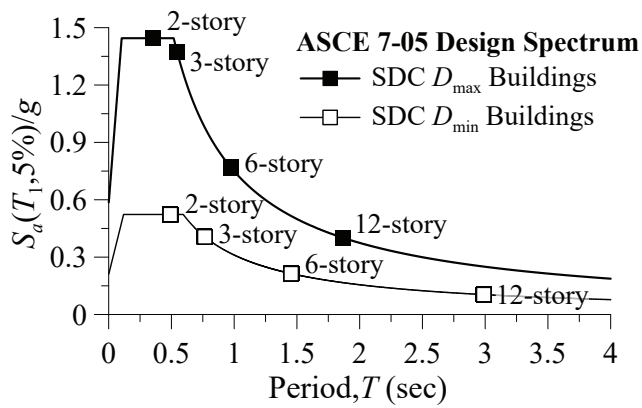
2.  $D_{min}$

$S_{DS} = 0.5g, S_{D1} = 0.3g$

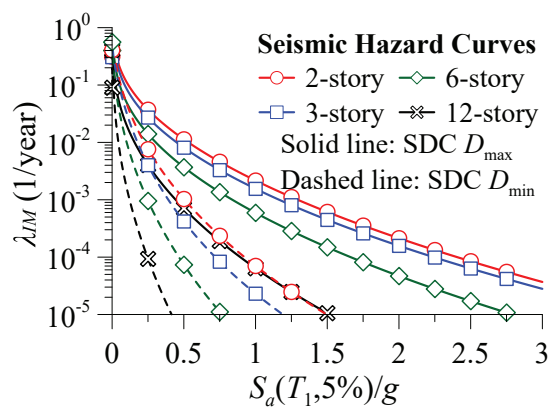
$F_a = 1.3, F_v = 1.8$

Sacramento, California

**FIG. 1 Archetype steel-frame buildings with perimeter SCBFs: (a) typical plan view; and (b) elevation view of the 3-story SCBF**

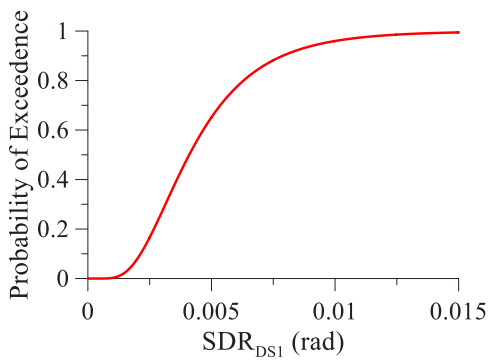


(a) Design spectrum

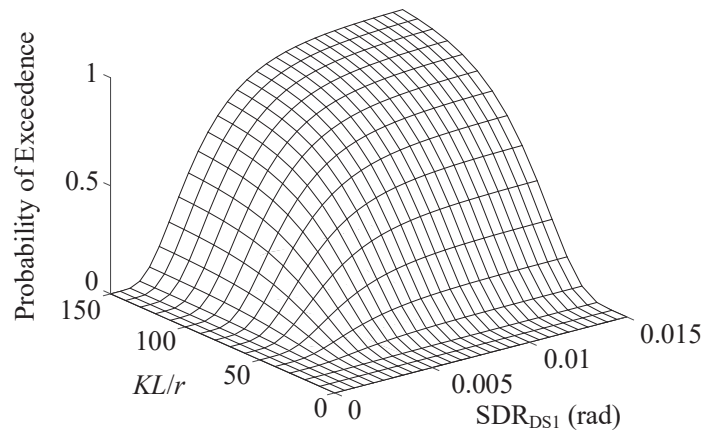


(b) Site-specific seismic hazard curves

**FIG. 2 Design spectrum and site-specific seismic hazard curves for bare model representations of archetype buildings with SCBFs**



(a) Univariate fragility curve



(b) Dual-parameter fragility curve

**FIG. 3 Example of fragility curves for damage state of global buckling for round HSS braces: (a) univariate fragility curve; and (b) dual-parameter (global slenderness  $KL/r$ ) fragility curves [adopted from Lignos and Karamanci (2013)]**

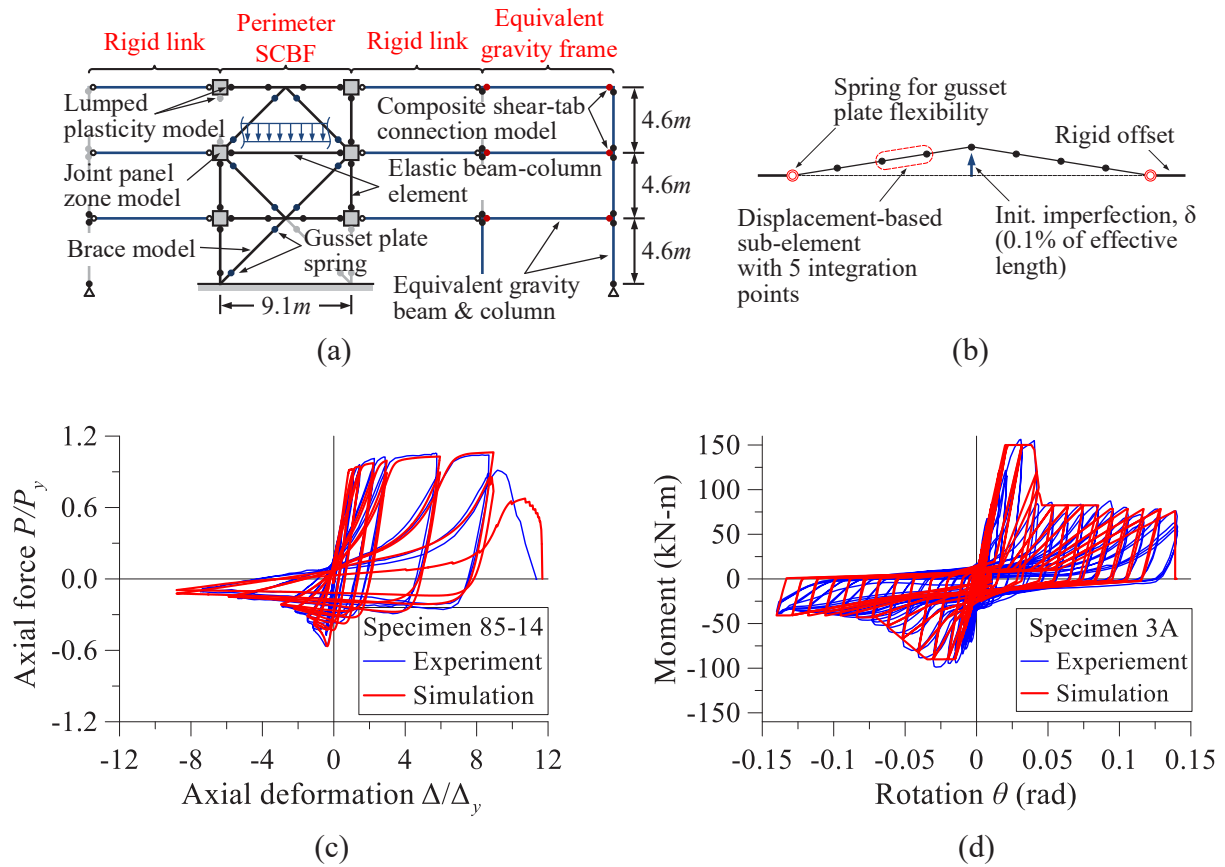


**FIG. 4 Analytical model representation of steel-frame buildings with SCBFs: (a) 2-D analytical model including the gravity framing (CG model); (b) description of the steel brace component model; (c) axial force-deformation relation for rectangular HSS brace section [data from Han et al. (2007)]; and (d) moment-chord rotation relation for composite beam in single-plate shear tab connections [data from Liu and Astaneh-Asl (2000)]**

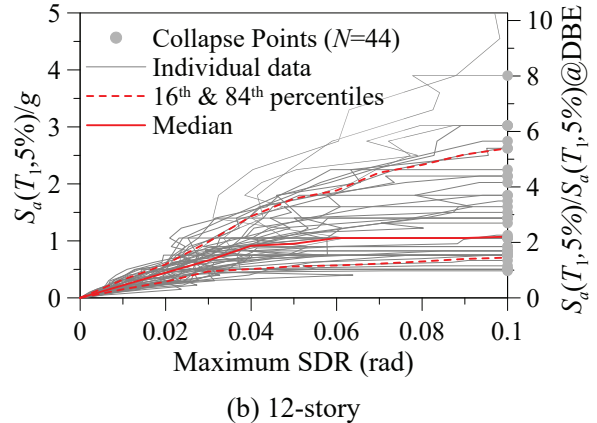
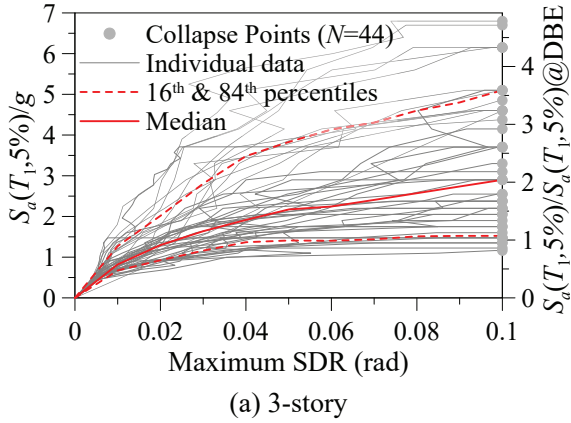


**FIG. 5 IDA curves for the 3- and 12-story steel-frame buildings with perimeter SCBFs (CG models)**

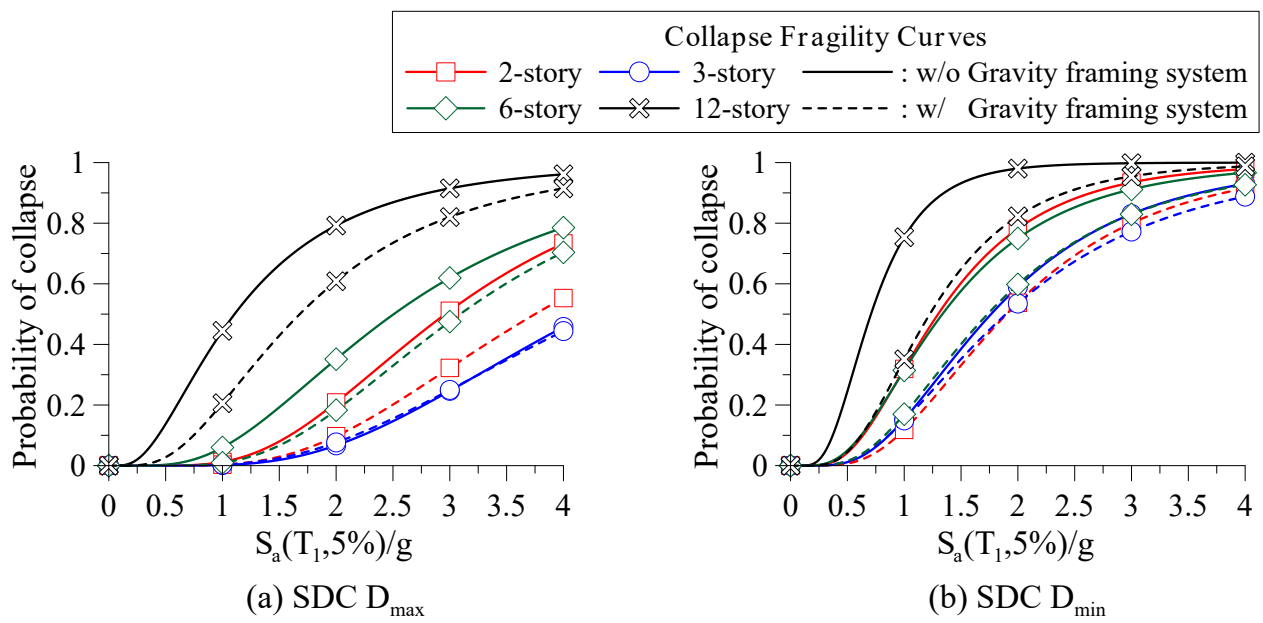


**FIG. 6 Collapse fragility curves for steel-frame buildings with perimeter SCBFs with/without gravity framing system**

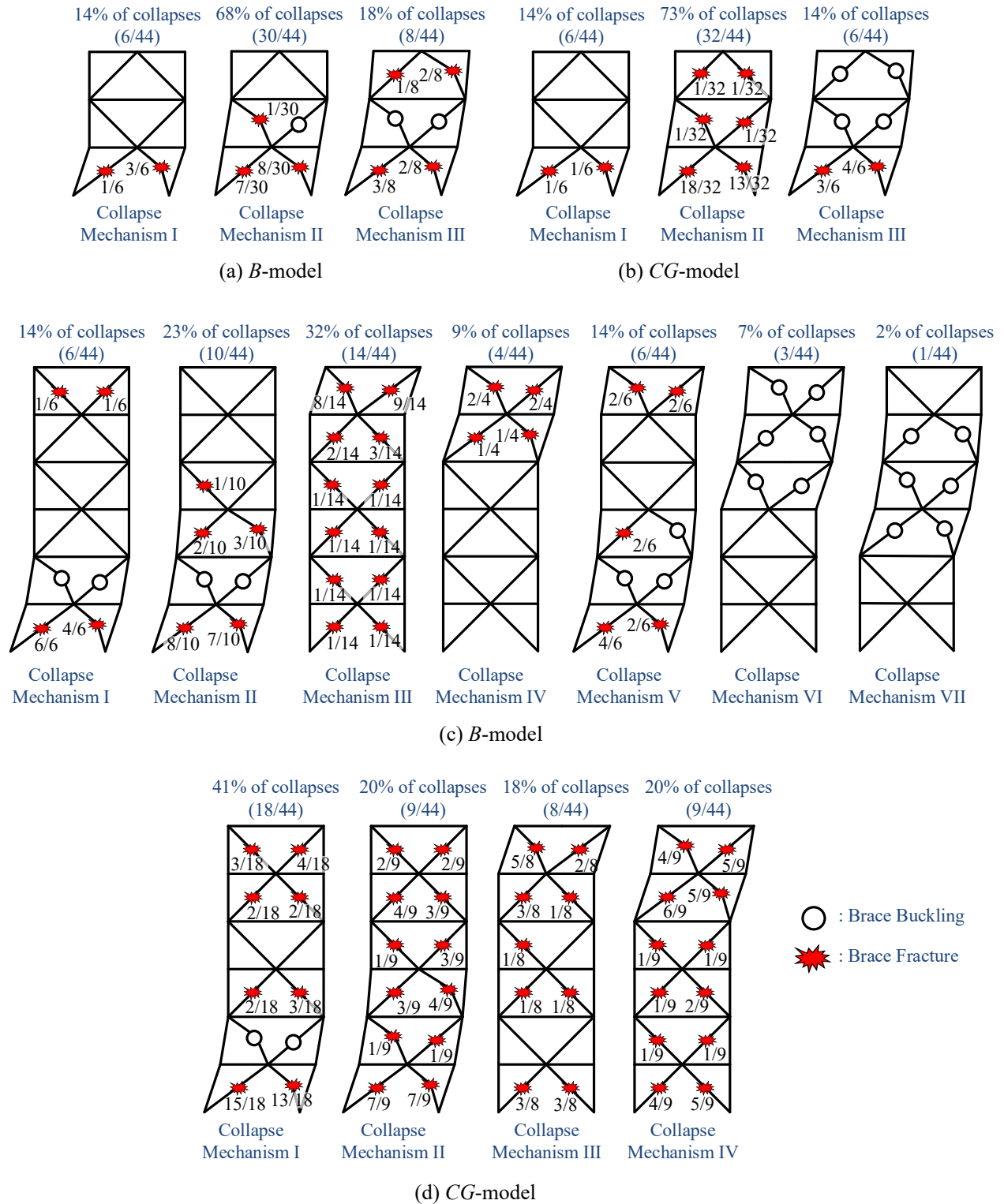


**FIG. 7 Collapse mechanisms for the 3- and 6-story archetypes based on B and CG models**

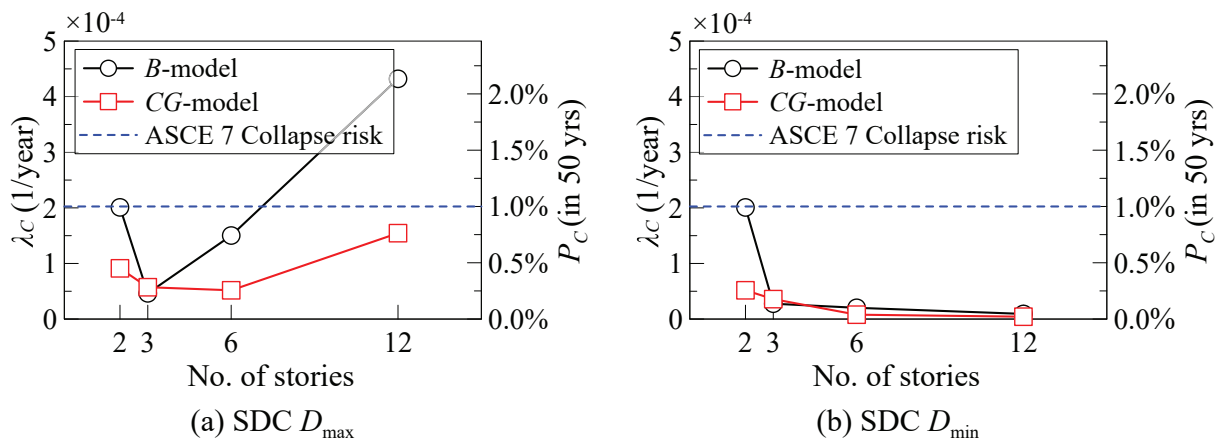


**FIG. 8 Mean annual frequency of collapse  $\lambda_c$  and the corresponding collapse probability over 50 years  $P_c$  (in 50 years) for the analytical model type of archetype buildings with perimeter SCBFs**



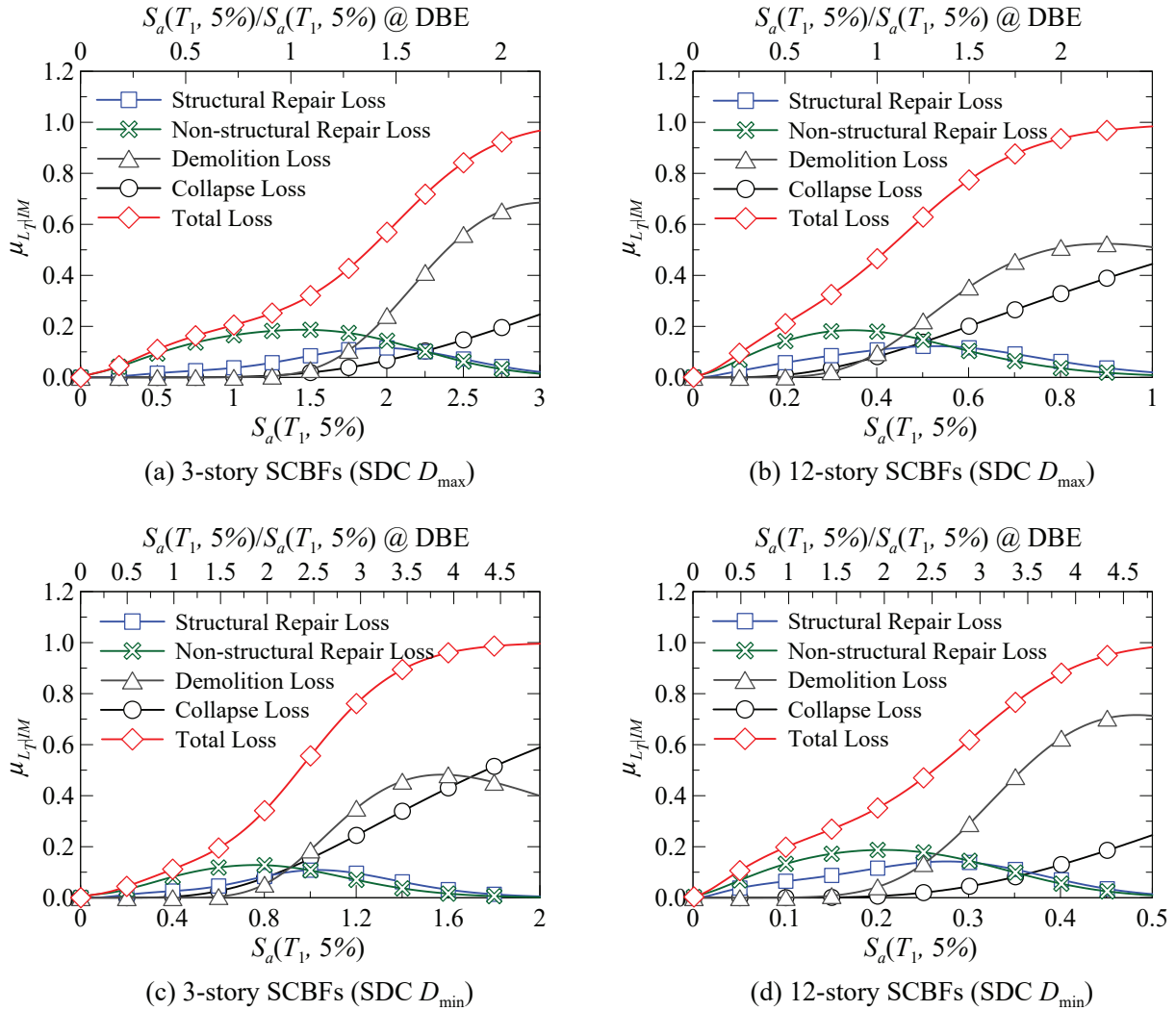


**FIG. 9 Normalized loss vulnerability curves for steel-frame buildings with perimeter SCBFs designed for SDC  $D_{max}$  and  $D_{min}$  conditioned on seismic intensity**

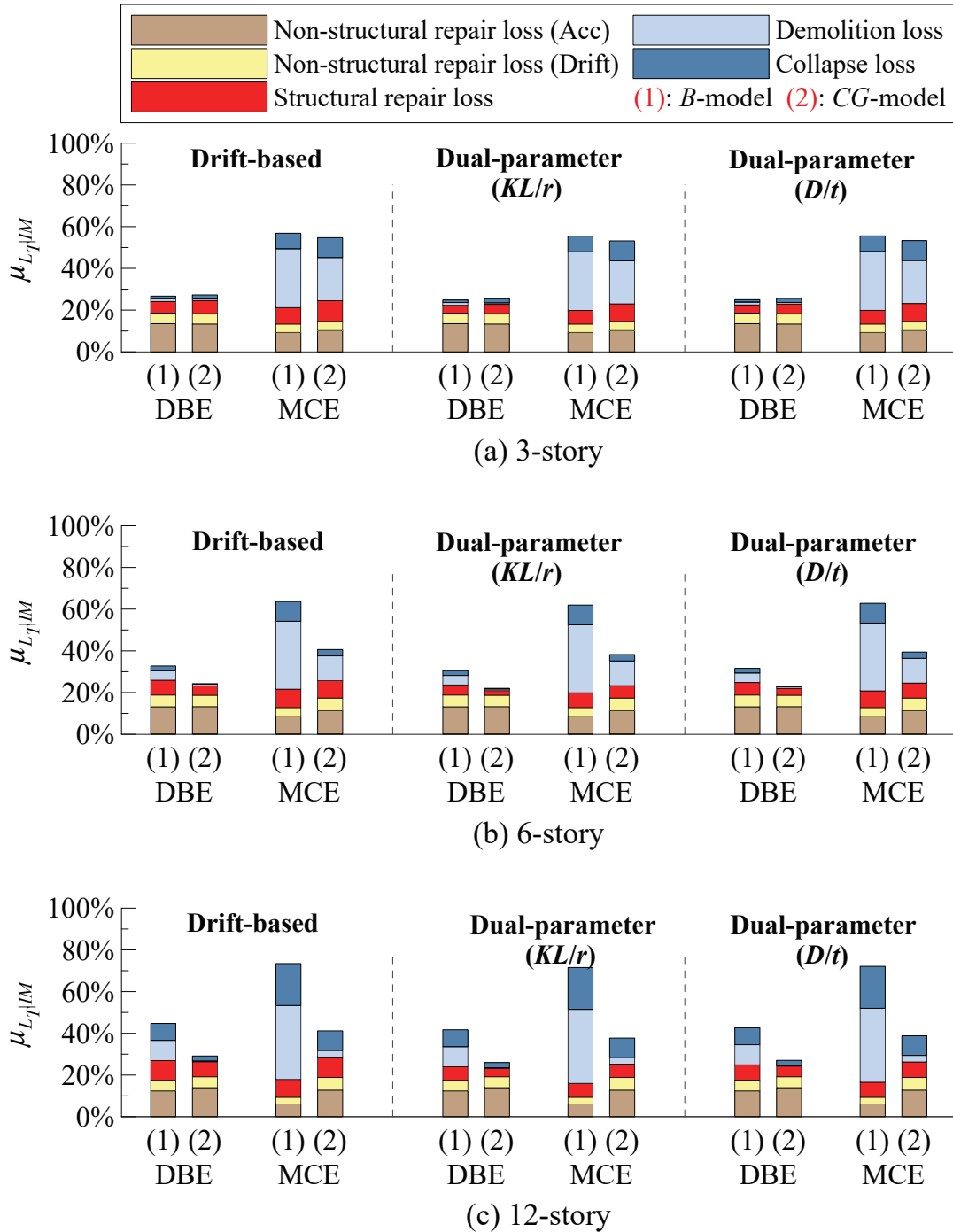


**FIG. 10 Normalized expected losses of steel-frame buildings with perimeter SCBFs designed for SDC  $D_{max}$  conditioned on selected seismic intensities**

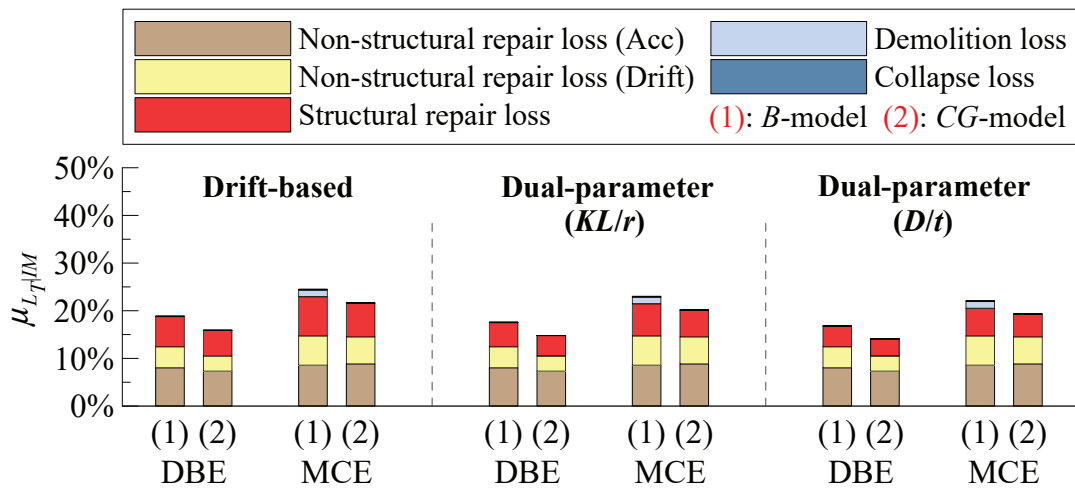


**FIG. 11 Normalized expected losses of the 12-story steel-frame building with perimeter SCBFs designed for SDC  $D_{min}$  conditioned on selected seismic intensities**

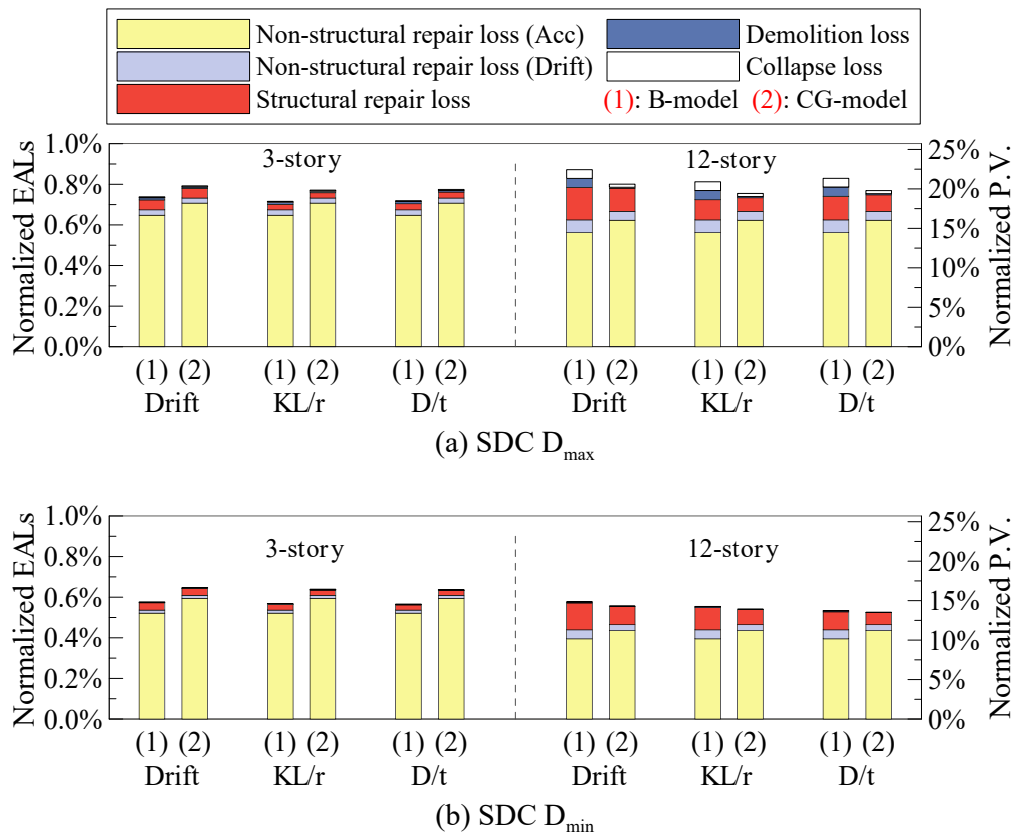


**FIG. 12 Normalized expected annual losses and present values for steel-frame buildings with SCBFs**